Journal Name

ARTICLE

Flexible Zn- and Li-Air Batteries: Recent Advances, Challenges, and Future Perspectives

Received 00th January 20xx,
Accepted 00th January 20xx

DOI: 10.1039/x0xx00000x

www.rsc.org/

Peng Tan[a], Bin Chen[a], Haoran Xu[a], Houcheng Zhang[a,f], Weizi Cai[a], Meng Ni[a,b*], Meilin Liu[c], Zongping Shao[d,e*]

The demand for flexible power sources with high energy density and durability increases rapidly with the development of flexible and wearable electronic devices. Metal-air batteries are considered as the most promising candidates for these applications due to their excellent theoretical energy densities. In particular, rechargeable zinc-air and lithium-air batteries have attracted much attention because of their potential to offer a high energy density while maintaining a long operational life. Although significant progress has been made in enhancing the electrochemical performance of these batteries, many technical challenges still remain to achieve the mechanical flexibility required for wearable electronic devices while maintaining high performance. This article describes the most recent advances and challenges in the development of flexible zinc-air and lithium-air batteries. We start with an overview of the latest innovations in the exploration of various battery configurations to effectively accommodate stresses and strains associated with the use of flexible electronic devices. This is followed by a detailed review of the advancements made in designs of flexible battery components: the metal electrode, the electrolyte membrane, and the air electrode. Further, the effects of operating conditions on battery performance characteristics and durability are discussed, including the effects of the operating temperature and the contaminants commonly encountered in ambient air (e.g., carbon dioxide and moisture). Finally, challenges facing the development of a new generation of flexible metal-air batteries are highlighted, together with further research directions and perspectives.

1. Introduction

Flexible electronic devices have gained increasing popularity recently. In contrast to the well-developed rigid format, the flexible devices can be bent, twisted, rolled, or stretched to a certain extent but still maintain their functions.[1] They not only bring revolution to the traditional electronic industrial with new concepts and opportunities (e.g., roll-up displays),[2,3] but also represent a promising area in healthcare when combined with wearable sensors (e.g., smart wristbands).[4,5] Accompanied with the development of flexible electronic devices, flexible energy storage systems have become a major research area.[6] Lithium-ion batteries (LIBs), due to their reasonable theoretical energy density (~400 Wh kg^{-1}), cycle life (>5000 cycles), and energy efficiency (>90%),[7] have been recognized as the energy sources in flexible electronic devices.[8–12] However, their energy densities hardly satisfy the requirements of advanced electronic devices for a long duration. Therefore, the exploitation of new energy storage technologies with higher energy densities is still a grand challenge.[13]

Compared to batteries with closed systems such as LIBs, metal-air batteries (MABs) have attracted great attention recently, since they possess a unique half-open system that uses the oxygen from ambient air, minimizing the required mass and volume of the air electrode and increasing the energy density.[14] Different from the intercalation mechanism of LIBs, the working mechanisms of metal-air batteries involve the metal dissolution and deposition on the negative (or metal) electrode and oxygen reduction reaction (ORR) and oxygen evolution reaction (OER) on the positive (or air) electrode. The theoretical capacities, energy densities, and cell voltages of various metal electrodes in MABs are shown in **Fig. 1**. Based on the applied electrolytes, MABs can be typically divided into aqueous and aprotic systems.[15] Zinc (Zn)-air, aluminum (Al)-air, and magnenism (Mg)-air batteries are compatible with aqueous alkaline electrolytes and have been studied for a long time. Although Al-air and Mg-air batteries have theoretical capacities up to 10 times higher than those of LIBs,[16] their low practical voltages due to the large polarization lead to the low energy densities. In addition, they can hardly be electrochemically charged in alkaline electrolytes, limiting their application as secondary batteries.[17] Comparatively, Zn is more stable and can be charged more efficiently in an alkaline electrolyte.[18] Besides, a Zn-air battery (ZAB) as a theoretical energy density (1218 Wh kg^{-1}) of about three

[a] *Department of Building and Real Estate, The Hong Kong Polytechnic University, Hung Hom, Kowloon, Hong Kong, China.*
[b] *Environmental Energy Research Group, Research Institute for Sustainable Urban Development (RISUD), The Hong Kong Polytechnic University, Hung Hom, Kowloon, Hong Kong, China.*
[c] *School of Materials Science and Engineering, Center for Innovative Fuel Cell and Battery Technologies, Georgia Institute of Technology, Atlanta, GA 30332-0245, USA.*
[d] *Jiangsu National Synergetic Innovation Center for Advanced Material, College of Energy, State Key Laboratory of Materials-Oriented Chemical Engineering, Nanjing Tech University, Nanjing 210009, China.*
[e] *Department of Chemical Engineering, Curtin University, Perth, WA 6845, Australia.*
[f] *Department of Microelectronic Science and Engineering, Ningbo University, Ningbo 315211, China.*
* Corresponding authors:
Email: zongping.shao@curtin.edu.au; (Prof. Zongping Shao)
Email: meng.ni@polyu.edu.hk; Tel: 852-27664152 (Prof. Meng Ni)

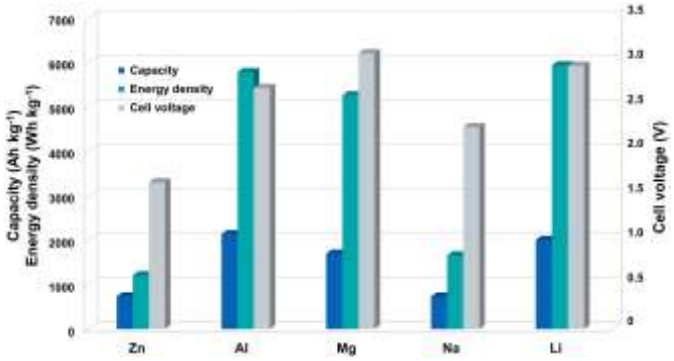

Fig. 1 Theoretical capacities, energy densities, and cell voltages of various metal electrodes in metal-air batteries. Theoretical capacities and energy densities account for oxygen uptake in the battery by numerical integration between the initial and discharged stages (data from ref. 18).

times higher than that of LIBs but with a lower manufacture cost.[19] Hence, ZABs have been regarded as great promise to replace LIBs for future energy applications.[20]

The basic structure of a ZAB is schematically shown in **Fig. 2a**, which is composed of a zinc electrode, an alkaline electrolyte, and a porous air electrode with active materials. Although room-temperature ionic liquids (RTILs) have also been applied in ZABs, their relatively high viscosity and low conductivity substantially restrict the electrochemical performance.[21] So we focus on the aqueous-based ZABs in this article. During discharge, the oxidation of zinc occurs, liberating the electrons that travel through an external circuit to the air electrode. Meanwhile, atmospheric oxygen molecules diffuse into the air electrode and are reduced through ORR to form hydroxide ions (Eq. 1) at the three-phase boundaries among oxygen (gas), electrolyte (liquid), and active material (solid). The generated hydroxide ions migrate to the zinc electrode, forming zincate ions ($Zn(OH)_4^{2-}$) (Eq. 2), which further decompose to insoluble zinc oxide (ZnO) (Eq. 3) when becoming supersaturated in the electrolyte. The diffusion of zincate ions from the metal electrode to the air electrode gives rise to an increased polarization and decreased cycling efficiency. To this end, a separator may be used between the two electrodes to allow the flow of hydroxide ions while blocking the zinc ions.[20] The overall reaction is summarized in Eq. 4, with an equilibrium potential of 1.65 V.

Air electrode: $O_2 + 4e^- + 2H_2O \rightarrow 4OH^-$ (1)

Zinc electrode: $Zn + 4OH^- \rightarrow Zn(OH)_4^{2-} + 2e^-$ (2)

$Zn(OH)_4^{2-} \rightarrow ZnO + H_2O + 2OH^-$ (3)

Overall reaction: $2Zn + O_2 \rightarrow 2ZnO$ ($E_{OCV} = 1.65$ V) (4)

To electrochemically charge the battery, the aforementioned electrochemical reactions are reversed, in which zinc is deposited at the zinc electrode and oxygen is released through OER at the electrolyte-electrode interface. Although primary ZABs have been

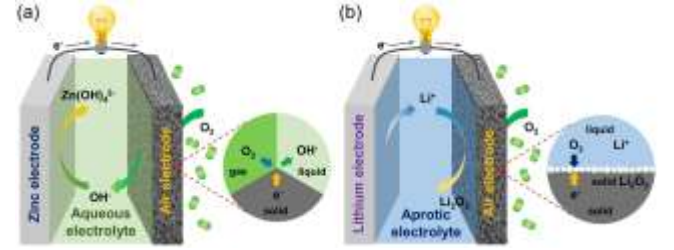

Fig. 2 Schematic operation principle of (a) Zn-air battery and (b) Li-air battery.

commercialized since the 1930s and successfully implemented for medical applications (e.g., hearing aids),[22] the development of rechargeable ZABs is still in the early stages with several critical issues that should be addressed such as the zinc dendrite and the low energy efficiency (<60%) due to the lack of bi-functional catalysts.[23]

Different from Zn-air, Al-air, and Mg-air batteries, sodium (Na) and lithium (Li) react strongly with an aqueous electrolyte. Consequently, these two types of batteries are initially based on aprotic electrolytes.[15,24,25] Due to the highest theoretical energy density (5928 Wh kg^{-1}) and the high cell voltage (2.96 V), Li-air batteries (LABs) have attracted worldwide attention since the demonstration of a prototype rechargeable LAB in 1996.[26] With the use of solid-state lithium ion conducting electrolytes, aqueous electrolytes based LABs (i.e., aqueous, hybrid aprotic/aqueous) and solid-state LABs have also been developed,[27] whereas the aprotic system is the most widely developed one owing to its highly reversible capacity,[28] and also be focused in this article. Similar to the ZAB, a typical LAB consists of a lithium metal electrode, a porous air electrode with active materials, and an aprotic electrolyte made of an aprotic solvent dissolved with a lithium salt, as schematically shown in **Fig. 2b**. To avoid the internal short-circuit between the anode and the cathode, a separator may be implemented between two electrodes. During discharge, lithium metal is oxidized at the electrode, producing electrons and lithium ions (Eq. 5); while atmospheric oxygen molecules dissolve first into the aprotic electrolyte, and then are reduced through ORR at the two-phase boundaries between electrolyte (liquid) and active material (solid) to form superoxide ions (Eq. 6).[29] The superoxide ions combine with lithium ions transported via the electrolyte to form lithium superoxide (LiO_2), which subsequently undergo a one-electron-transfer electrochemical process (Eq. 7a) and/or a disproportionation reaction (Eq. 7b) to form lithium peroxide (Li_2O_2). Different from zincate ions which can be dissolved in the aqueous electrolyte, Li_2O_2 has limited solubility in the aprotic electrolyte and deposits on the surface of the air electrode.

Lithium electrode: $Li \rightarrow Li^+ + e^-$ (5)

Air electrode: $O_2 + e^- \rightarrow O_2^-$ (6)

$LiO_2 + Li^+ + e^- + \rightarrow Li_2O_2$ (7a)

$2LiO_2 \rightarrow Li_2O_2 + O_2$ (7b)

Total reaction: $2Li + O_2 \rightarrow Li_2O_2$ ($E_{OCV} = 2.96$ V) (8)

During charge, the electrochemical process is reversed, producing lithium and releasing oxygen. Attributed to the ten times higher theoretical energy density than that of state-of-the-art LIBs, LABs have been advocated as the promising power sources for electric vehicles (EVs).[30] Although great progress has been achieved with tremendous efforts in recent decade, a wide variety of technical hurdles still need to be overcome to make LABs commercially viable, such as the low obtainable discharge capacity, poor energy efficiency, and limited cycle life.[31] In addition, LABs are highly sensitive to moisture and carbon dioxide and are usually tested in pure oxygen instead of ambient air;[32] accordingly, they are also called "Li-O_2" batteries in most previous reports.[32] In this article, we still use the term of "Li-air", but the reported battery performances were acquired under oxygen atmosphere unless specified.

In light of their high theoretical energy densities, ZABs and LABs are regarded as the most promising technologies among various energy storage systems.[15] Some excellent reviews have been published on the respective advances of ZABs and LABs,[7,33–38], covering the reaction mechanisms,[39–44] battery components,[13,17,45–49] and the whole system.[18,50–52] With an increasing interest in flexible electronic devices, developing flexible energy storage

systems have attracted great research attention, which requires to not only overcome the technique barriers in electrochemical performance (e.g., low energy efficiency, short cycle life), but also satisfies the new challenges in deformation (e.g., bending, twisting). Focusing on flexible LIBs and flexible supercapacitors (SCs), breakthroughs have been achieved in recent years, including fabricating effective electrode and electrolyte materials for improved electrochemical performance,[53–57] and designing novel configurations for high flexibility and durability.[58–60] In addition, it has emerged a number of excellent reviews on state-of-the-art flexible batteries and SCs.[61–68] For example, Lu *et al.* summarized the achievements in the design, fabrication, and characterization of flexible SCs, and discussed the challenges and opportunities for performance improvements.[64] Fu *et al.* reviewed the structural design and material design of flexible batteries for wearable electronics, from which the mechanics and design concepts are also crucial for other flexible energy storage systems.[67] Mao *et al.* focused on the mechanical deformation characterization, analysis, and structural design strategies in flexible LIBs and SCs for practical applications, and the key parameters in mechanical evaluation were highlighted.[68] Different from LIBs and SCs, MABs are half-open systems associated with pure metals and oxygen from ambient air.[69] Hence, developing flexible MABs will induce more challenges and require more research efforts. In 2016, Sumboja *et al.* presented a review on the advancements in flexible MABs.[70] Several types of polymer electrolytes for alkaline Zn- and Al-air batteries were summarized, and carbon- and conducting polymer-based flexible air cathodes were reviewed. Besides, two prototype flexible devices, including the sandwich and cable structures, were outlined. Nevertheless, with increasing research activity in flexible energy storage systems, an up-to-date review of the current status and challenges of flexible MABs, covering the battery configuration design, the flexible electrode and electrolyte materials, and the operation managements, has become highly necessary.

In this article, we focus on the latest progress and challenges of flexible ZABs and LABs for adapting flexible requirements and achieving high electrochemical performance. The aim of this work is to provide a timely snapshot of the rapidly developing area of flexible MABs. Although these two types of batteries represent the aqueous and aprotic systems, respectively, they share a number of similarities when made into flexible batteries. We start with an overview of the latest innovations in the exploration of various battery configurations to effectively accommodate stresses and strains associated with the use of flexible electronic devices, followed by a detailed review of the advancements made in designs of flexible battery components: the metal electrode, the electrolyte membrane, and the air electrode. Further, the effects of operating conditions on battery performance characteristics and durability are discussed, including the effect of the operating temperature and the contaminants commonly encountered in ambient air. Finally, challenges facing the development of a new generation of flexible metal-air batteries are highlighted, together with further research directions and perspectives.

2. Battery configuration and flexibility evaluation

For the application in flexible electronic devices, a stable electrochemical performance during the repetitive external force is crucial for flexible MABs. To this end, a novel configuration of the battery is required to enable high electrochemical and mechanical stabilities. In this section, different configurations of flexible MABs are introduced, and the related flexibility evaluations are also discussed.

2.1 Sandwich type

One kind configuration of flexible MABs is the sandwich type, as schematically illustrated in **Fig. 3**.[18] The metal electrode (e.g., Zn) is attached to a metal (e.g., Cu) foil as a substrate/current collector to ensure good electrical contact. Then, an electrolyte membrane is sandwiched between the metal electrode and the air electrode. A porous current collector is attached to the air electrode for gas diffusion and electrons transfer.

Due to its high similarity to that of conventional ones, the sandwich type structure has been widely used in flexible ZABs and LABs, and good electrochemical performance has also been achieved as summarized in **Table 1**. For example, Fu *et al.* developed a flexible solid-state ZAB that reached a peak power density and energy density as high as 160.7 mW cm^{-2} and 847.6 W h kg_{Zn}^{-1}, respectively. The battery could be cycled for over 500 h at 25 mA cm^{-2} without visible voltage losses.[72] Liu *et al.* reported a LAB with a high discharge capacity of ~9500 mAh $g_{cathode}^{-1}$ and a cycle life up to 72 cycles (720 h) at a fixed capacity of 1000 mAh $g_{cathode}^{-1}$.[84]

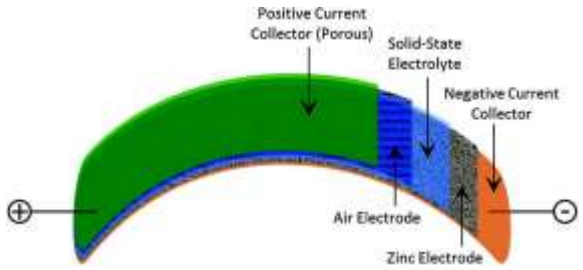

Fig. 3 Schematic configuration of a sandwich-type zinc-air battery. Reprinted with permission from ref. 18, copyright 2017, Wiley-VCH.

Table 1 Summary of sandwich-type Zn- and Li-air batteries

Battery type	Rechargeability	Electrochemical performance	Flexibility evaluation	Ref.
Zn-air	Yes	Capacity: 460 mAh $g_{Zn\ film}^{-1}$ Energy density: 581 Wh kg^{-1} Cyclability: 120 cycles at 50 mA g^{-1} (20 min per cycle)	120 cycles at 50 mA g^{-1} at bending angles of 90°, 150°, and 180°	71
	Yes	Peak power density: 160.7 mW cm^{-2} Capacity: 652.6 mAh cm^{-2} Energy density: 847.6 W h kg_{Zn}^{-1} Cyclability: over 500 h at 25 mA cm^{-2} (20 min per cycle)	Voltage polarization curves remained unchanged at bending angles of 60°, 90°, and 120°; Power a light-emitting diode (LED) under flat and bent conditions.	72
	Yes	Peak power density:[a] ~1900 mW g_{Zn}^{-1}	Power density almost remained unchanged at bending angles of 60°, 90°, and 120°	73

	Yes	Capacity: 378 mAh g_{Zn}^{-1} Energy density: 378 Wh kg_{Zn}^{-1} Cyclability: 12 cycles at 2 mA cm^{-2} (10 min per cycle)	Discharge-charge curves remained unchanged when applying bending strain every 2 h	74
	N/A	Capacity: 144 mAh cm^{-2} Energy density: 682 Wh kg_{Zn}^{-1}	Discharge voltage remained unchanged when bending	75
	N/A	Capacity: 353.9 mAh g_{anode}^{-1} Energy density: 363.4 mWh g_{anode}^{-1}	Photograph showed the bendability	76
	Yes	Peak power density:[a] ~50 mW cm^{-2}	Voltage polarization curves remained unchanged at bending angles of 60°, 90°, and 120°; Power density changed little.	77
	Yes	Peak power density: 97.8 mW cm^{-2} Cyclability: 12 h at 100 mA cm^{-2} (10 min per cycle)	Charged and discharged at bending angles of 120° and 180°	78
	Yes	Peak power density: 32.0 mW cm^{-3} Capacity: 603.7 mAh g_{Zn}^{-1} Cyclability: 28 h at 12.5 mA cm^{-3} (40 min per cycle)	Galvanostatic discharge voltages remained unchanged under different deformation conditions	79
	Yes	Peak power density: [a] ~20 mW cm^{-2} Cyclability: 10 h at 2 mA cm^{-2} (20 min per cycle)	Discharge-charge curves remained unchanged at different bending radius (13, 28, 51 mm); No obvious changes in the discharge curve at a bending radius of 28 mm for 300 cycles; Brightness of a flexible display remained virtually unchanged under various bending and twisting conditions.	80
	Yes	Capacity: 356 mAh g^{-1} Energy density: ~382 Wh kg^{-1}	Discharge-charge curves remained unchanged at bending angles of 60°, 90°, 120°, and 150°.	81
	Yes	Capacity: 6500 mAh $g_{cathode}^{-1}$ Cyclability: 50 cycles at 200 mA g^{-1} (1000 mAh g^{-1})	Capacity, rate, first discharge-charge curves, and cycle number almost remained unchanged after 1000 folding cycles	82
	Yes	Cyclability: over 140 cycles at 0.4 mA cm^{-2} (1000 mAh $g_{composite}^{-1}$)	Overpotential greatly increased after 10 cycles under the bending condition	83
	Yes	Capacity:[a] ~9500 mAh $g_{cathode}^{-1}$ Cyclability: 72 cycles at 200 mA g^{-1} (1000 mAh g^{-1})	A LED turned on with planar and bent conditions.	84
	Yes	Capacity: 3000 mAh $g_{cathode}^{-1}$ Cyclability: 356 cycles at 100 mA g^{-1} (1000 mAh g^{-1})	100 stable cycles (500 mAh g^{-1}) at bending angles of 180°, 360° and twisting angles of 90°, 180°, and 360°	85
	Yes	Cyclability: 10 cycles at 0.10 mA cm^{-2} (1000 mAh g^{-1}) Rate: Stable discharge-charge curves at 0.02, 0.05, and 0.10 mA cm^{-2}	A LED turned on with planar and bent conditions.	86
Li-air	Yes[b]	Capacity: 7111 mAh $g_{cathode}^{-1}$ Energy density: 2540 Wh $kg_{cathode+product}^{-1}$ Cyclability: over 180 cycles at 1000 mA g^{-1} (500 mAh g^{-1})	Discharge voltage plateau maintained when: i) stretching with a strain up to 100%; ii) at the bending angles of 45°, 90°, 135°, and 180°; iii) at the twisting angles of 90°, 180°, 270°, and 360°. Discharge voltages maintained after stretching, bending, and twisting for 1000 cycles each.	87
	Yes	Capacity: 9017 mAh $g_{cathode}^{-1}$ Cyclability: over 210 cycles at 200 mA g^{-1} (500 mAh g^{-1})	Discharge voltage curves and capacities almost remained unchanged in different shapes (pristine, bend, roll up) and even after 5000 folding cycles; 100 stable cycles after 1000 bending, folding, and rolled up cycles each; Open-circuit voltage remained almost unchanged after bending for 5000 cycles.	88

[a] Estimated from the figure; [b] Operated in ambient air with the relative humidity (RH) of ~5%.

In addition to the basic electrochemical performances, the flexibility evaluations are crucial for flexible MABs. Based on the direction of the external force, three kinds of deformation are usually considered: bending, twisting, and stretching. The bendability is basically demonstrated through measuring the discharge/charge voltages[75] or powering an electronic equipment (e.g., LED) under the bending conditions.[84,85] In more detailed tests, the electrochemical performances (e.g., polarization, power density, cycle stability) at different bending angles are measured and compared with the initial ones under the planar condition to show the stability.[71–73,77,78,85,87] Similarly, the twistability is evaluated by measuring the electrochemical performances under different twisting angles.[85,87] Although the stretchability has few been considered in the flexible sandwich-type battery, partial stretching also occurs in the battery components during bending and twisting processes, which may affect the performance and even damage the structure.[71] Hence, unique configurations were designed and tested in which the discharge curves were well maintained after the stretching-induced strain reached 100%.[87] Besides the short-term deformation, a long-term fatigue test is important. For instance, Zhang *et al.* showed that a flexible LAB could maintain the capacity, rate performance, first discharge-charge curves, and cycle number after 1000 folding cycles.[82] Peng *et al.* developed a flexible LAB that maintained the discharge voltage after stretching, bending, and twisting for 1000 cycles each.[87]

2.2 Cable type

Another configuration of flexible MAB is the cable type, as schematically shown in **Fig. 4**.[89] It contains a metal electrode in the centre, which is wrapped by an electrolyte membrane (e.g., gel polymer). The catalyst loaded air electrode is then winded on the polymer electrolyte. To enhance the surface contact between electrodes and the electrolyte, a heat-contraction rubber cable is applied to pack the electrode assembly, and the punched holes act as air pathway.

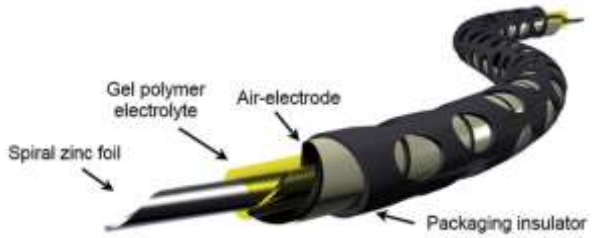

Fig. 4 Schematic configuration of a cable-type Zn-air battery. Reproduced with permission from ref. 89, copyright 2015, Wiley-VCH.

Due to the high omnidirectional flexibility,[70] the cable type flexible ZABs and LABs have gained research interest, as summarized in **Table 2**. Zhang *et al.* fabricated a cable-type ZAB that could maintain a discharge voltage plateau of ~1.23 V at a current density of 0.5 mA cm^{-2} and a standing time as long as 15 h.[91] Besides, 36 cycles (12 h) with stable voltage plateaus were realized at a constant current density of 0.5 mA cm^{-2}. Moreover, this type of battery delivered stable discharge performance at different bending and twisting conditions and even after 2000 bending/stretching cycles, demonstrating a good stability. The excellent performance

Table 2 Summary of cable-type Zn- and Li-air batteries

Battery type	Rechargeability	Electrochemical performance	Flexibility evaluation	Ref.
Zn-air	N/A	Energy density: 3.6 Wh $L_{battery}^{-1}$	Discharge voltage profiles remained the same between the bending and non-bending conditions every 20 min from initial length of 7 to 3 cm	89
	Yes	Capacity: 6 Ah $L_{battery}^{-1}$ Energy density: 5.7 Wh L^{-1} Cyclability: 30 cycles at 1 mA g^{-1} (1 h per cycle)	No obvious damage in structure when bent to 30°, 60°, 90°, 120°, and 150°; Discharge voltage remained almost unchanged before and after: i) bending to 120° for 100 cycles; ii) stretching by 10%.	90
	Yes	Capacity:[a] ~10 mAh cm^{-2} Cyclability: 36 cycles at 0.5 mA cm^{-2} (20 min per cycle)	Discharge voltage remained almost unchanged at bending angles of 30°, 60°, 90°, and 120°; Discharge curve only suffered from a very slight drop of ~13 mV after 2000 cycles of bending/stretching	91
Li-air	Yes	Capacity:[a] ~3.1 mAh cm^{-2} Cyclability: over 109 cycles at 0.1 mA cm^{-2} (0.1 mAh cm^{-2})	A LED display screen was powered at various bending and twisting conditions.	91
	Yes[b]	Capacity: 13055 mAh g_{CNT}^{-1} (O_2) 12,470 mAh g_{CNT}^{-1} (Air) Cyclability: over 100 cycles at 500 mAh g^{-1} (O_2) 30 cycles at 1000 mAh g^{-1} (Air)	Discharge curves were maintained under increasing bending angles of 30°, 45°, 60°, 90°, 120°, and 145°; Voltage profiles were almost unchanged after bending for 100 cycles; Operating stably under a dynamic bending and releasing process at a speed of 10° per second.	92

Yes	Capacity:[a] ~4750 mAh $g_{cathode}^{-1}$ Cyclability: over 90 cycles at 100 mA g^{-1} (500 mAh g^{-1})	Discharge curves remained constantly and powered a LED display screen under all the testing conditions (linear, arc-shaped, rounded, s-shaped, twisty, and spiral); Discharge-charge curves kept almost unchanged after 4000 cycles of bending/stretching.	93
Yes[c]	Capacity: 1262 mAh g_{total}^{-1} (1981 mAh g_{carbon}^{-1}) Cyclability: 100 cycles at 200 mA g^{-1} (600 mAh g^{-1})	A LED turned on at bending, knotting, and releasing conditions; Charge and discharge curves remained unchanged for 100 cycles at the bending condition.	94

[a] Estimated from the figure; [b] Operated in pure oxygen and ambient air with the RH of 5%; [c] Operated in pure oxygen with the RH of 8 %.

has also been achieved in cable-type LABs. Peng *et al.* developed a flexible LAB that could not only deliver a capacity as high as 13055 mAh g_{CNT}^{-1} but also showed a long cycle life up to over 100 cycles at 1400 mA g^{-1}.[92] In addition, the discharge curves were maintained under increasing bending angles, and the voltage profiles were almost unchanged after bending for 100 cycles. Similar to the flexibility evaluation in sandwich-type batteries, besides the bending, twisting, and long-term fatigue tests, the stretchability could also be achieved through unique design. For example, a ZAB could deliver a stable discharge voltage even at an elongation of 10%.[90]

2.3 Other types

In addition to the sandwich and cable types, other types of flexible MABs with innovative ideas have also been designed. A foldable LAB pack was fabricated based on a paper-ink air electrode, as schematically shown in **Fig. 5a**.[82] An inexpensive flexible paper served as the substrate of the air electrode, the separator, as well as the outer package, enabling the assembled battery to be foldable and bendable. In addition, the lithium electrodes wrapped into the paper could be shared by two air electrodes, improving the utilization of lithium and the energy density of the battery.

Inspired by the ancient Chinese bamboo slips, which were fabricated using bamboo chips and hide ropes that can be rolled up easily, a flexible and wearable LAB was developed by Zhang *et al.* (**Fig. 5b**).[95] The lithium electrodes and air electrodes are woven together, similar to the "bamboo chips" and "hide ropes" in bamboo slips. With this assembly structure, the battery can maintain its electrochemical performance in various bending, twisting, and folding conditions, demonstrating excellent flexibility. In addition, the woven structure has a unique property of allowing gas access to the air electrode via both sides of the weave, endowing good gas breathability for the battery. Moreover, lithium electrodes are protected by a polypropylene (PP) membrane and a hydrophobic gel polymer electrolyte (GPE), avoiding the sudden hazards posed by moisture or water so that the assembled battery can operate even immersed in water. Attributed to the sophisticated structure design that avoids using packing materials, the energy density of this battery can be as high as 523.1 Wh kg^{-1}, which is far beyond the values of commonly commercial LIBs.[96] They also built a novel segmented Li-air battery that consisted of arrays of small-scale carbon electrode disks and lithium electrode disks interconnected by carbon ropes and copper wires, respectively.[97] This special structure enabled the battery to demonstrate a superior flexibility and electrochemical stability even after 10,000 cycles of folding and stretching, and achieved a high gravimetric and volumetric energy density of 294.68 Wh kg^{-1} and 274.06 Wh L^{-1}, respectively.

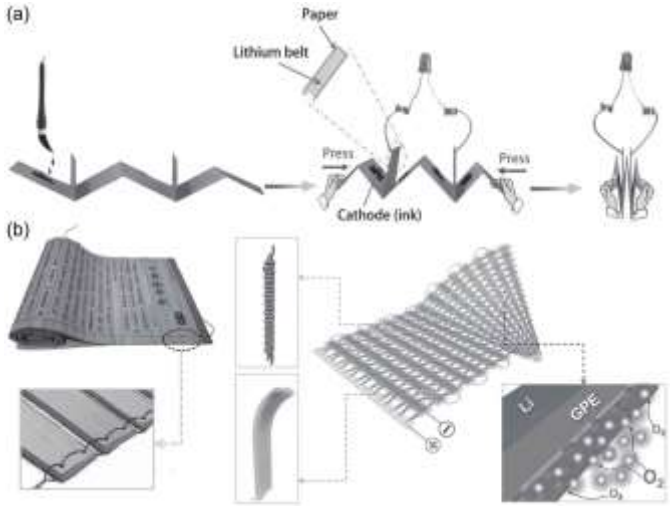

Fig. 5 (a) Schematic configuration of a foldable Li-air battery pack. Reproduced with permission from ref. [82], copyright 2015, Wiley-VCH. (b) A flexible and wearable Li-air battery inspired by the ancient bamboo slips. Reproduced with permission from ref. 95, copyright 2016, Wiley-VCH.

Although different configurations are developed for flexible ZABs and LABs and some promising performance has been achieved, several issues should be addressed for further development. First of all, in ZABs the capacity and energy density are normalized to the zinc electrode (g_{Zn}^{-1}) or the surface area (cm^{-2}); while these values in LABs are normalized to the mass of the air electrode ($g_{cathode}^{-1}$), resulting in encouraging but misleading results.[20] Hence, even though flexible ZABs and LABs share similar battery configuration (e.g., sandwich and cable types), a direct comparison of the respective electrochemical performance is difficult at the present stage. Besides, even for the same kind of battery, the electrochemical performance in different battery configurations was reported from different bases. For example, the energy densities in sandwich-type ZABs were usually based on the mass of the zinc electrode (**Table 1**), while in cable-type ZABs the energy densities were reported based on the total volume of the battery (**Table 2**). The different standards lead to difficulties in systematically estimating the feasibilities of different configurations. Moreover, the flexibilities are evaluated case by case, while a recognized standard is still absent. Usually, the flexibility evaluations include measuring the electrochemical performance under different bending/twisting angles and after bending/stretching cycles, as well as powering an electronic device (e.g., LED) under deformation conditions. To commercialize the flexible MABs, a critical testing standard should be made and used

in the following works, such as the bending/twisting angles, the elongation levels, and the performance retention after long-term deformation cycles. Since the development of flexible MABs is in its infancy stage, more innovative ideas in both flexible configuration and evaluation methods are highly demanded. In the following parts, we will mainly focus on the design and challenges of battery components to satisfy the flexibility while maintaining the electrochemical performance.

3. Metal electrode

Metallic Zn and Li pieces are usually directly used in MABs as metal electrodes. To design fully flexible devices, modifications to the metal electrodes are needed. For instance, electrodeposited Zn on carbon cloth instead of pure Zn foil was applied to make the battery with improved flexibility.[79] Stainless steel mesh, Li foil, and Cu foil were rolled together to fabricate a high-fatigue-resistance electrode that can maintain its structure even after 300 bending cycles.[88] In this section, we review some approaches in the design of flexible metal electrode. The free-standing metal composite electrodes with improved stabilities in bending and twisting are first introduced. Then, the unique designs of metal electrodes for satisfying the requirements of stretching are also summarized.

3.1 Free-standing composite electrode

A free-standing zinc composite electrode was reported by Fu *et al.*,[71,73] which was made of a combination of zinc powder, carbon nanofiber (CNF), carbon black (CB), and poly(vinylidene fluoride-co-hexafluoropropylene) (PVDF-HFP) as the binder. As illustrated in **Figs. 6a-c**,[71] the free-standing zinc film can be freely rolled, twisted, and folded without any mechanical damages, which is attributed to the excellent distribution of zinc particles through building up a three-dimensional (3D) interconnected network with carbons and the binder (**Figs. 6d-e**), where the carbons help to enhance the electrical conductivity of the 3D zinc film electrode. In addition, the binder can not only ensure a short curing time but also avoid the oxidation of zinc particles. Mitra *et al.* mixed zinc powder, polymer binder, bismuth oxide, and purified multi-walled carbon nanotubes (MWCNTs) to form the anode,[76] and found that MWCNTs were effective conducting additive in anode as they bridged the zinc particles, and poly(3,4-ethylenedioxythiophene):polystyrene sulfonate (PEDOT:PSS) acted as a co-binder to enhance both the conductivity and flexibility.

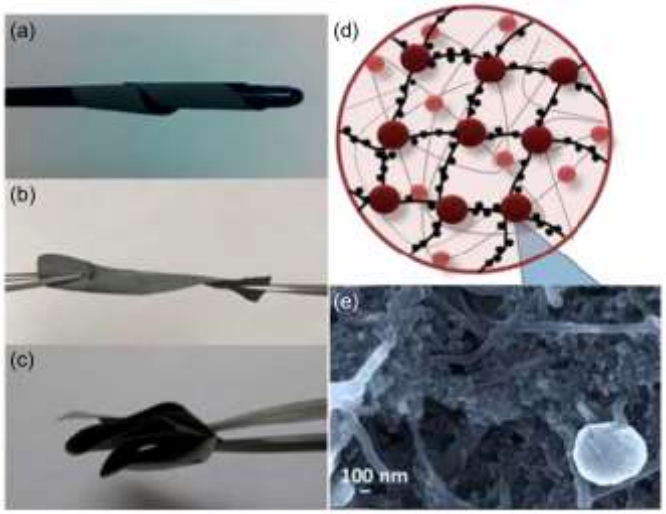

Fig. 6 The digital pictures of the free-standing zinc film under (a) rolled, (b) twisted, and (c) folded state. (d) A schematic and (e) SEM image of the 3D interconnected electrical conducting network with carbon nanofiber, carbon black, and zinc particle. Reproduced with permission from ref. 71, copyright 2015, Wiley-VCH.

3.2 Modification of metal piece

In the sandwich-type flexible batteries, to make the lithium electrode stretchable, Peng *et al.* designed a lithium array electrode based on a stretchable copper (Cu) current collector, as schematically shown in **Fig. 7a**.[87] First, the Cu springs made of a Cu wire were connected in series by Cu sheets. Then, lithium sheets were paved on the Cu sheets point-to-point and covered by a punched Ecoflex film. This stretchable metal electrode associated with gel electrolyte and rippled air electrode enabled a good stretchability of the battery, which could maintain the discharge voltage plateau with a strain up to 100%. This "break up the whole into parts" strategy has also been applied in Liu's work, in which the lithium electrode disks are interconnected by carbon ropes and copper wires.[97] With this unique structure, the whole segmented lithium metal electrodes could almost keep unchanged even after folded in half and then stretched up to 1000 cycles. In contrast, the whole piece of lithium metal sheets cracked after only 100 folding and stretching cycles.

To satisfy the requirement of stretching, a zinc spring electrode was used in a cable-type Zn-air battery, as schematically shown in **Fig. 7b**.[90] It was first prepared by coiling a zinc wire onto a steel rod. After removing it from the rod, the zinc spring was then dipped into a hydrogel polymer electrolyte and decorated with catalysts. Then, the modified zinc spring was rolled on the prepared Teflon plate covered by the carbon nanotube (CNT) sheet air electrode, which served as both the current collector and the gas diffusion layer. With this spring metal electrode, the discharge voltage of this flexible battery could remain almost unchanged after stretching by 10%. The spring-like zinc electrode was also applied in Zhang's work, in which the discharge curve of a cable-type ZAB only suffered from a very slight drop of ~13 mV even after 2000 cycles of bending and stretching.[91]

As both Zn and Li metallic pieces have good flexibility to some extent, little attention has been paid to metal electrodes in flexible MABs. However, the use of metallic piece will introduce some issues such as the low contact area and utilization, limiting the electrochemical performance. In addition, the continuous bending/stretching cycles will easily lead to the metal fatigue,

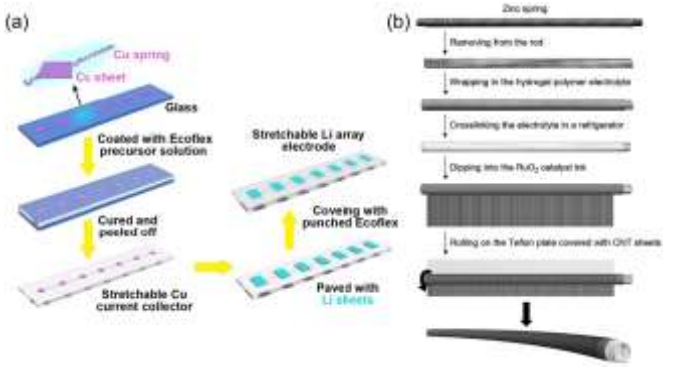

Fig. 7 Schematic illustration of the fabrication of (a) a stretchable Li array electrode for a sandwich-type LAB. Reproduced with permission from ref. 87, copyright 2016, The Royal Society of Chemistry. (b) a cable-type ZAB with a Zn spring electrode. Reproduced with permission from ref. 90, copyright 2016, Wiley-VCH.

resulting in the mechanical failure of the metal electrode. To this end, using high surface area metal particles associated with conductive networks and binders to form a free-standing electrode is expected for better electrochemical performance and mechanical stability.[20] Moreover, the dendrite formation and growth during cycling are common phenomena in both metal electrodes and are detrimental to the battery performance and safety. This issue will be discussed in detail in Section 4.3.1.

4. Electrolyte membrane

In some flexible battery prototypes, the porous separators (e.g., glass fibre paper) saturated with liquid electrolytes were used between the metal and air electrodes.[91] However, evaporation and leakage are two critical issues for the liquid electrolytes. Moreover, the use of flammable organic liquid electrolytes in LABs leads to a major safety concern for practical applications. To this end, solid-state electrolytes provide a feasible solution to these issues. They can function as both electrolytes for ion conduction and separators for preventing the battery internal short-circuiting. Consequently, we use "electrolyte membrane" to describe the roles in conducting and separating. The main required properties include high ionic conductivity and selectivity, a wide electrochemical stability window, good chemical compatibility with other components, and excellent mechanical properties.[98,99] To be applied in flexible MABs, an excellent flexibility is also essential. During past decades, great efforts have been contributed to developing electrolyte membranes to improve the safety and reliability of the batteries. In this section, we first introduce the electrolyte membranes that have been applied or demonstrated promising potentials for flexible ZABs and LABs, respectively. Then, challenges for the electrolyte-electrode interfaces are discussed.

4.1 Electrolyte membranes for flexible Zn-air batteries

Alkaline anion-exchange membranes, which impregnate basic functional groups into a polymer backbone with a single phase, have been developed and widely applied to alkaline fuel cell applications.[100,101] Although they can conduct hydroxide ions during battery operations and prevent zinc ion migration from reaching the air electrode, the ionic conductivities are limited for the application of ZABs. In addition, the water retaining property is poor, resulting in a rapid water loss by evaporation when operated in the air atmosphere, and thus leads to a fast degradation of ionic conductivities and battery performance.[73] Another kind of solid-state electrolyte membrane is made by dissolving alkaline salts into an inert polymer matrix.[102] Although the solution-free electrolytes can be built into a thin film with sufficient mechanical strength, the ionic conductivities (typically 10^{-5} to 10^{-8} S cm^{-1} at room temperature) are below the requirements for battery applications.[103] An alternative approach to enhance the ionic conductivity is to encapsulate aqueous alkaline electrolytes in polymeric matrix to form an alkaline gel electrolyte (AGE).[104–108] The AGE membranes exhibit good aqueous electrolyte absorbing capabilities, facilitating the hydroxide-ion conduction and reaction kinetics. However, the mechanical properties are usually inadequate for practical use.[103] In Sumboja's work, several types of alkaline solid and gel polymer electrolytes have been summarized.[70] Here we centre on introducing the electrolyte membranes used in recently reported flexible ZABs.

4.1.1 Alkaline gel electrolyte membrane

Poly(vinyl alcohol) (PVA) has been widely used as the host polymer for AGEs. The generally fabrication process is adding PVA and KOH into water to form a uniform solution, followed by pouring the solution onto a glass plate. After equilibrated at a low temperature, a robust electrolyte membrane is obtained for battery.[74,78,91] In addition to using PVA alone, other host materials, such as N-vinyl-2-pyrrolidone, vinyl imidazole, and glycidyl methacrylate, have also been used to form the polymer solution.[79] To further improve the mechanical properties of the AGE, Peng *et al.* added poly(ethylene oxide) (PEO) during the fabrication process (**Fig. 8a**). As shown in **Figs. 8b-c**, the cross-linked electrolyte was free-standing, flexible and stretchable with a maximal strain of 300%, and showed high ionic conductivity of 0.3 S cm^{-1} with 8.3 wt% KOH (**Fig. 8d**), which was close to the KOH solution with the same concentration.[90] With this AGE, a cable-type flexible ZAB displayed excellent discharge and charge performance at a high current density of 2 A g^{-1} and also could be stretched by 10% with a stable discharge voltage.

To ensure leak-free solid-type behaviour, Cho *et al.* developed a new highly conductive AGE based on gelatin with a lower concentration of KOH (0.56 wt%). The fabrication procedure involves dissolving gelatin powder in KOH solution, followed by a frozen process. At the optimized concentration of KOH solution (0.1 M), a free-standing AGE membrane was obtained, which not only showed a high flexibility but also demonstrated an ionic conductivity of 3.1 mS cm^{-1}, enabling reasonably high discharge capacities at 0.1, 0.5, and 1 mA cm^{-2} in a cable-type flexible ZAB.[89]

4.1.2 Alkaline-exchange electrolyte membrane

Based on cellulose, Chen *et al.* developed a thin, ultra-flexible and hydroxide conductive electrolyte membrane with high water retention for ZABs.[72,73] The cellulose nanofibers are composed of a variety of micron-sized cellulose fibers and fine fibrils with lengths of over several hundred microns, which have a greatly expanded surface area. The membrane surface appears as a homogenous and dense nanofiber network intertwined with the micron-sized fibers functioning as the strong ''scaffold'', giving the membrane a very

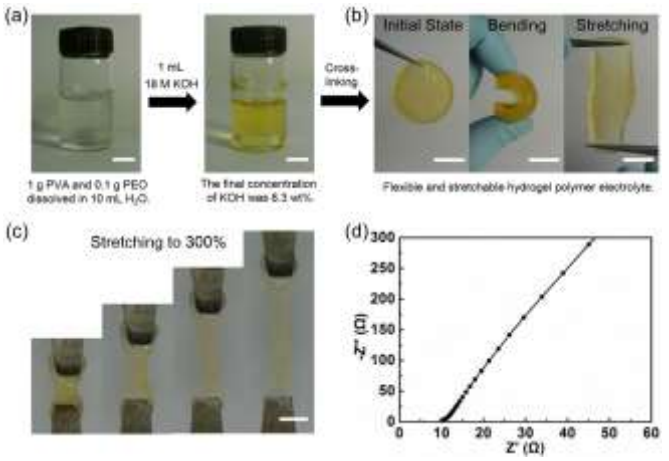

Fig. 8 Preparation and characterizations of hydrogel polymer electrolyte: (a) Photographs of synthetic process of hydrogel polymer electrolyte solution, scale bar: 1 cm. (b) Photographs of free-standing hydrogel polymer electrolyte after crosslinking, scale bar: 1cm. (c) Photographs of hydrogel polymer electrolyte in a stretching process up to 300%, scale bar: 0.5 cm. (d) Alternating current (AC) impedance spectra of the hydrogel polymer electrolyte at the frequency range from 1000 kHz to 0.01 Hz. Reprinted with permission from ref. 90, copyright 2015, Wiley-VCH.

strong mechanical property and excellent flexibility. Owing to the interconnected nanoporous structure, the membrane exhibited a high water uptake up to 95.6% and moderate anisotropic swelling degree of 1.1. Benefiting from the dissociated hydroxide ions from quaternary ammonia functional groups, the membrane exhibited a high ionic conductivity of 21.2 mS cm^{-1}.[73]

Graphene oxide (GO) has been demonstrated as a promising candidate for solid-state electrolytes due to its outstanding physicochemical stabilities and electrochemical properties. Based on GO and cellulose, Chen *et al.* reported a laminate-structured nanocellulose/GO membrane functionalized with highly hydroxide-conductive quaternary ammonium (QA) groups.[77] The QA-functionalized nanocellulose/GO (QAFCGO) membrane is fabricated through chemical functionalization, layer-by-layer filtration, cross-linking, and ion-exchange processes, as schematically shown in **Fig. 9a**. After vacuum filtration, the water-based suspensions of QA-functionalized GO nanosheets and cellulose nanofibers form a laminate-structured membrane (**Fig. 9b**) supported by QA-functionalized GO at the top and bottom with a flat and uniform surface (**Fig. 9c**). The numerous cellulose nanofibers tend to construct a dense interwined porous network (**Fig. 9d**), and perform as binder layers to integrate each single thin GO film into a robust membrane. Finally, after the ion exchange process, the hydroxide-conducting QAFCGO membrane is obtained with excellent flexibility as shown in **Fig. 9e**, and a superior hydroxide conductivity of 58.8 mS cm^{-1} at 70 °C was achieved. With this flexible QAFCGO membrane, a sandwich-type flexible ZAB delivered an output power density up to 50 mW cm^{-2} under stress at different bending angles.

4.2 Electrolyte membranes for flexible Li-air batteries

Solid-state lithium-ion conducting materials have attracted great attention recently and been considered as underlying electrolytes for lithium-based batteries.[109,110] For ceramics, such as

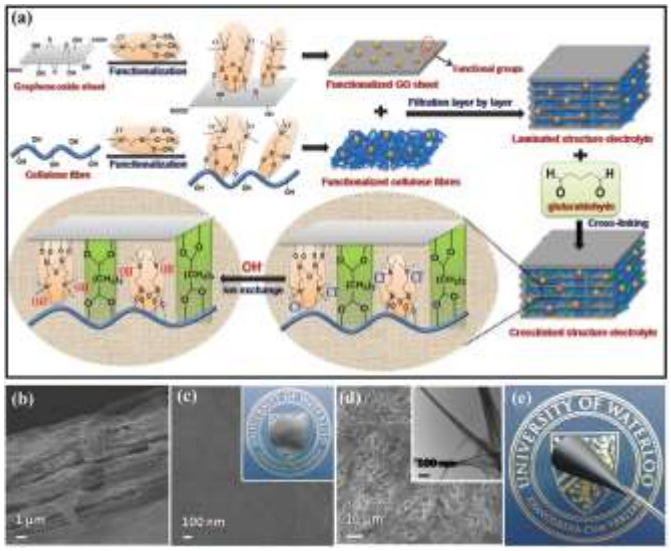

Fig. 9 (a) Schematic diagram of the overall preparation procedure of functionalization, filtration, cross-linking, and hydroxide-exchange for the QAFCGO membrane. (b-c) SEM images of (b) cross section and (c) surface view of the QAFCGO membrane, inset shows the photograph of QAFCGO membrane with flat and uniform GO surface. (d) A SEM image of the cellulose dense interwined network structure with an inset TEM image of cellulose fibres. (e) A photograph of the QAFCGO membrane showing flexibility. Reprinted with permission from ref. 77, copyright 2016, Wiley-VCH.

$Li_{1+x}Al_xTi_{2-x}(PO_4)_3$ (LATP) and $Li_{1+x}Al_xGe_{2-x}(PO_4)_3$ (LAGP),[111–113] although they display a high ionic conductivity (>10^{-4} S cm^{-1}) and good chemical and electrochemical stabilities, the fragile property inhibits their application in flexible batteries.[114] Consequently, polymer electrolyte serves as a better candidate due to good processability and mechanical strength.[115] The polymer electrolyte can be divided into three classes:[109] GPEs, solid polymer electrolytes (SPEs), and composite polymer electrolytes (CPEs). Similar to AGEs applied in ZABs, the GPE in lithium-based batteries is to encapsulate aprotic electrolytes in a polymeric matrix. In SPEs, the polymer host together with a lithium salt act as a solid solvent. The CPEs are developed by the integration of inorganic fillers into the organic polymer host.

4.2.1 Gel polymer electrolyte membrane

One approach to fabricating GPEs is preparing the porous membranes with polymer matrix first and then immersing in an aprotic electrolyte before use. Wu *et al.* reported lithiated perfluorinated sulfonic (PFSA-Li) single-ionic conducting ionomers swollen with aprotic solvents and used as both the electrolyte and separator for LABs.[116] In addition to using polymer matrices, different types of inorganic nanofillers have also been added to form hybrid GPEs to improve their properties. For instance, ZrO_2 nanoparticles are added in the poly(vinylidene fluoride) (PVDF)-based polymer matrix to improve the mechanical strength;[117,118] nanofumed SiO_2 with poly(methyl methacrylate)-blend-poly(styrene) were coated on a commercial microporous PP separator to enhance the ionic conductivity;[119] amorphous $LiNbO_3$ with low grain boundary resistance were combined with poly(methyl methacrylate-styrene) to achieve a high Li-ion conductivity of 0.26 mS cm^{-1} at room temperature.[114]

Adding liquid aprotic electrolytes into the polymer matrix is also applied in the fabrication process of GPEs that can be directly used in batteries. Generally, the solid PVDF-HFP is dissolved in a solvent (e.g., acetone, N-methyl-2-pyrrolidone (NMP)), and the liquid aprotic solvent and lithium salt are added. The homogeneous solution is then cast onto a flat surface to allow the solvent to evaporate, and eventually, a dimensionally stable, flexible, and free-standing GPE can be obtained.[120,121] In addition to PVDF-HFP, PEO has also been added to improve the mechanical strength for stretchability.[87] Besides the solution casting method, ultraviolet (UV) irradiation has also been used for fabricating GPEs.[83,92,93] For example, three kinds of solutions were mixed together, including i) lithium triflate ($LiCF_3SO_3$) in tetraethylene glycol dimethyl ether (TEGDME), ii) PVDF-HFP in NMP, and iii) 2-hydroxy-2-methyl-1-phenyl-1-propanon (HMPP, photo-initiator) in trimethylolpropane ethoxylate triacrylate (TMPET). After UV irradiation, a solidified and flexible GPE was obtained with a high ionic conductivity of 1.15×10^{-3} S cm^{-1} at 25 °C. The GPE in a cable-type flexible LAB prevents air diffusion to the lithium electrode and alleviate its corrosion for high cyclic stability in air, enabling an excellent electrochemical performance and stability.[92]

4.2.2 Solid polymer electrolyte membrane

Compared to the above-mentioned solid-state electrolytes in which liquid aprotic electrolytes may still exist, SPEs have the liquid-free property and have been regarded as the most promising candidate electrolytes for solid-state lithium-based batteries.[109] The studies of SPEs started from the incorporation of PEO with lithium salts, in which lithium ion cations were solvated by the polymer chains and became movable through the chain movement.[122] For LABs, Ein-Eli *et al.* used PEO and $LiCF_3SO_3$ with a composition of $P(EO)_{20}LiTf$,

followed by a solution casting technique, to achieve a free standing and homogeneous GPE with a thickness of ~150 µm. It could function as the electrolyte at 80 °C for the ionic conductivity that is comparable to the common organic electrolyte.[123] Besides PEO, polysiloxane has also been a candidate host, and the polysiloxane-based SPE displayed a relatively high conductivity (1.55×10^{-4} S cm^{-1} at 25 °C) due to the polysiloxane backbones and a good flexibility.[124]

4.2.3 Composite polymer electrolyte membrane

With the incorporation of inorganic materials, the properties of original SPEs may be greatly improved. As a result, CPEs have attracted many research interests. Byon *et al.* added SiO_2 into the PEO-based SPE to improve ionic conductivity, lithium interfacial stability, and mechanical strength. After the hot press, a homogeneous, flexible, and semi-transparent SPE was obtained with an ionic conductivity of 3.2×10^{-4} S cm^{-1} at 55 °C.[125] Fu *et al.* reported a 3D Li-ion-conducting ceramic network based on garnet-type $Li_{6.4}La_3Zr_2Al_{0.2}O_{12}$ (LLZO) lithium-ion conductor to provide continuous lithium ion transfer channels in a PEO-based composite, which exhibited an ionic conductivity of 2.5×10^{-4} S cm^{-1} at room temperature.[126] The schematic fabrication of fibre-reinforced polymer composite (FRPC) is shown in **Fig. 10a**, the Li salt-PEO polymer is reinforced by the 3D nanofibers to form a composite electrolyte. Compared with filler-containing polymer electrolyte, the FRPC electrolyte membrane maintains the framework of 3D garnet nanofiber networks. Attributed to the continuous nanofiber structure, the integrity of the polymer electrolyte could be enhanced, resulting in a better mechanical property and flexibility (**Fig. 10b**).

For these developed polymer electrolytes, the degradation of PEO-based SPE during the operation of Li-air batteries has been reported due to the superoxide attack.[125] Apart from PEO, most of the commonly used polymers, such as PVDF, PVDF-HFP, and poly(acrylonitrile) (PAN), are reactive and unstable in the presence of Li_2O_2.[116] Besides chemical instabilities, the high charge potential can also cause the decomposition of polymer electrolytes. For example, the oxidative decomposition of PEO-based polymer electrolyte starts around 4.5 V *vs* Li/Li$^+$, while a large potential is often observed during the charge processes (e.g., >4.5 V), resulting in a great threaten of the electrochemical stability.[127] To be commercially viable, the charge potential for LABs should be as low as possible (e.g., <3.5 V).[39] Hence, searching for effective catalyst materials to lower the charge potential still requires tremendous efforts.[128–130] Nevertheless, great attention should be paid to both chemical and electrochemical stabilities of polymer electrolytes, which are the prerequisite for the stable performance and long cycle life.

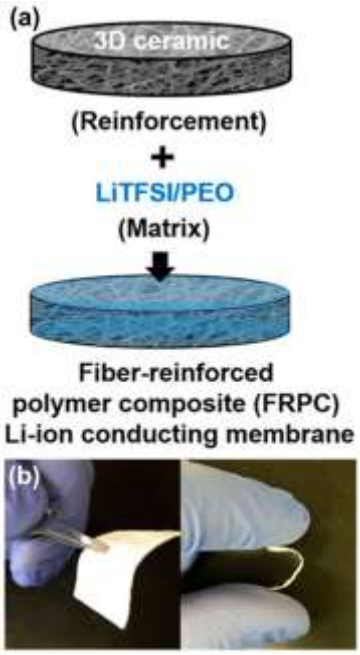

Fig. 10 Fabrication of the flexible solid-state FRPC electrolyte: (a) Schematic fabrication procedure. (b) Photo image to show the flexible and bendable of the membrane. Reproduced with permission from ref. 126, copyright 2016, National Academy of Sciences, USA.

4.3 Electrolyte-electrode interfacial issues

The electrolyte membranes can have the advantages of both high mechanical strengths of solids and high ion conductivities of liquids and thus are recognized as the best choice for flexible ZABs and LABs. However, the interfacial properties between the electrolyte and electrodes remain great challenging.

4.3.1 Metal electrode-electrolyte interface

The dendrites are critical issues for Zn- and Li-based batteries, which can fracture from the metal electrode, resulting in capacity losses;[18] or more seriously, can penetrate through the electrolyte membrane, leading to short-circuits.[131] Hence, with an increase of cycling, the dendrite will fade the electrochemical performance and even induce safety issues.[132]

Although zinc in alkaline electrolytes is highly reversible, its non-uniform dissolution and deposition usually result in the electrode shape change and/or dendritic growth. Different approaches have been attempted to mitigate these problems, such as coating the zinc metal and using additives in the zinc electrode and/or the electrolyte.[18,20] Different from alkaline solutions, polymer electrolytes appear to be useful in solving the zinc dendrite formation and growth.[133] Banik *et al.* used poly(ethylene glycol) (PEG) as an effective electrolyte additive to suppress dendrites during zinc electrodeposition. Results showed that the dendrite suppression efficiency increases with PEG concentration.[134] They also reported the use of branched polyethylenimine (PEI) as another electrolyte additive, through which the zinc electrodeposition kinetics is suppressed due to the PEI adsorption on the surface.[135] Besides using polymeric additives, Lee *et al.* developed a poly(acrylamide-co-acrylic acid) (P(AM-co-AA))-based AGE with a conductivity of 0.48 S·cm^{-1}. The zinc electrode with this AGE after 100 charge-discharge cycles showed only slight morphology change, demonstrating the effectiveness in suppressing dendrite formation.[136] Liu *et al.* developed an ionic liquid-based AGE with a good conductivity of 2.2 mS cm^{-1} and good mechanical stability.[137] More importantly, the morphology of the zinc deposits after 10 cycles of deposition/stripping is compact and dense without any dendrite formation, showing the promise of this AGE for rechargeable zinc-based batteries.

The uncontrollable dendritic lithium growth and limited Coulombic efficiency during deposition/stripping have prevented the applications of lithium electrode over the past 40 years.[138] In GPEs where the aprotic electrolytes contribute to the ionic conductivity, the dendrite growth may be mainly affected by the electrolyte composition.[139–141] It was proposed that the reduction potential of the solvent, the size of the salt anions, and the viscosity of the electrolyte are critical parameters for the rate of dendritic growth.[142] For instance, Choi *et*

al. found that the addition of 1,1'-pentyl-bis(2,3-dimethylimidazolium) bis(trifluoromethanesulfonyl)imide (PDMITFSI) instead of carbonate-based solvents lowered the interfacial resistance of the GPEs and mitigated the dendritic lithium formation, since PDMITFSI was used as a compatibilizer to modulate the electrolyte-rich phase for a lithium deposit pathway on the lithium metal anode.[143] In addition to the aprotic solvents, the polymer matrix can also affect the dendrite. It was reported that the GPEs with lower PAN concentrations suffered from reduced mechanical strength, while higher PAN concentrations resulted in increased bulk and interfacial resistance. With 5-17 wt% of PAN, the dendrite formation was suppressed in GPEs.[144]

The lithium dendritic growth in a PEO-based SPE has been reported by Brissot *et al*.[145–147] At a low current density (0.2 mA cm^{-2}), needle-like and particle-like dendrites were observed. While at higher current densities (e.g., 0.7 mA cm^{-2}), dendrites were not seen during the first polarization, but a compact metallic layer was formed instead. After several polarizations, dendrites were still observed with a tree-like or bush-like shape.[145] The dendrites induced a large change on the impedance component due to the unstable electrode-electrolyte interface, and even caused the short-circuits when reaching the opposite electrode.[148] Monroe and Newman investigated the relationship between dendrite formation and shear modulus, from which they proposed that for a polymer material with Poisson's ratio similar to PEO, the interfacial roughening is mechanically suppressed when the separator shear modulus is about twice that of lithium.[149] In a later study, Khurana *et al.* found that a cross-linked PE/PEO SPE with low-modulus (~1.0 × 10^5 Pa at 90 °C) could exhibit remarkable dendrite growth.[150] It is proposed that SPEs with shear moduli of the same order of magnitude as lithium could be used to suppress dendrite growth. Liu *et al.* added nano-SiO_2 filler into the PEO-based SPE and found that both the onset time of dendrite formation and the short-circuit time were extended in the formed CPE.[151] This may be attributed to the enhancement of the conductivity and the suppression of the interface resistance between lithium and the CPE by the addition of 10 wt% acid-modified nano-SiO_2. They further reported the amplification of this electrolyte system by the addition of *N*-methyl-*N*-propylpiperidinium bis(trifluoromethanesulfonyl)imide (PP13TFSI) to dramatically increase the onset time of dendrite formation from 15 to 46 h.[152] Archer *et al.* reported a facile and scalable method of fabricating tough and freestanding membranes that combine the best attributes of SPEs, GPEs, and nanocomposites.[153] PEO-tethered silica particles were linked with difunctional poly(propylene oxide) (PPO) to form the crosslinked nanoparticle-polymer composite in a desired macroscopic shape. The hydrophobic polymer provides a porous conductive pathway for Li-ion migration in a liquid electrolyte phase, while the short hydrophilic oligomer tethered to the nanoparticles provides structure and mechanical strength, achieving the effectiveness in inhibiting dendrite growth.

In addition to the above-mentioned dendrite issues, the passivation of the metal electrode is another critical issue. In ZABs, when a zinc electrode is discharged and the product $Zn(OH)_4^{2-}$ has reached its solubility limit, ZnO is precipitated on the metal electrode surface.[18] In LABs, the dissolved O_2, highly reactive intermediate species (such as superoxide radical), along with the side products from the electrolyte decomposition (e.g., H_2O) lead to serious contaminations of the lithium electrode, which causes the formation of a passivated film (e.g., LiOH) on the lithium electrode surface.[154] In both cases, the nonconductive ZnO and LiOH covering the metal electrodes will inevitably change the electrode-electrolyte interface, increasing the ion transport resistance, leading to performance degradation and even failure of the metal electrode.[18] Therefore, when associated with the electrolyte membranes, the metal electrode-electrolyte interface should be well maintained to achieve a high reversibility of the metal electrode.[131,155]

4.3.2 Electrolyte-air electrode interface

Besides the metal electrode-electrolyte interface, the electrolyte-air electrode interface seems to be more complicated. As schematically illustrated in **Fig. 11**, the catalysts at air electrodes have full access to the liquid electrolyte in traditional ZABs. In contrast, the three-phase boundaries are severely restricted in the solid configuration due to the poor wetting property of the "immobilized" electrolyte. Thereby, interfacial resistance to hydroxide ions transporting over the catalyst surface is substantially higher than that of the aqueous systems, leading to high overpotentials and undesirable low current rates during battery operation.[18] To solve this issue, developing microporous-structured solid electrolytes with a high hydroxide ion capacity and selectivity, as well as a strong mechanical property is crucial. For instance, Chen *et al.* demonstrated a quaternary ammonia-functionalized cellulose electrolyte membrane with an interconnected porous structure, which is critically important to retain a large degree of hydration for high ionic conductivity while maintaining dimensional stability in the water-swollen state of the membrane. Additionally, the uninhibited hydroxide ion availability to the electrodes facilitates the charge-transfer process at the air electrode during repeated cycles.[73]

The similar issue also exists in LABs with polymer electrolyte membranes.[156] Take the SPE as an example, as illustrated in **Fig. 12a**, the active reaction area where the gaseous oxygen, lithium ion, and electron can interact, is restricted to the topmost surface of the air electrode-electrolyte boundary. Hence, an improved SPE structure should have a large active reaction area along the longitudinal axis of the electrode for lithium ion transport, and meanwhile be reasonably thin in close proximity to the electrode to aid the smooth electron transfer to the gaseous oxygen (**Fig. 12b**). Byon *et al.* used a hot-pressing technique to establish the active reaction area by a thin coating of CNT with SPE and its integration into a 3D structure, which enhanced the capacity of the battery.[125] Zhou *et al.* developed an electrode made of lithium salt-modified single-walled CNTs and an ionic liquid-based cross-linked network gel and incorporated it into a LAB with a solid-state electrolyte.[157] Benefited from the 3D continuous passage of electrons, lithium ions, and oxygen supported by the electrode and the high lithium ion conductivity of the electrolyte, a stable electrolyte-air electrode interface was achieved, resulting in the improvement of cycling performance.[114]

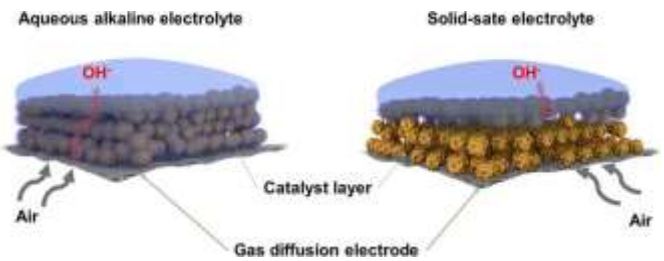

Fig. 11 Illustration of the three-phase boundaries in different types of electrolytes in Zn-air batteries. Reprinted with permission from ref. 18, copyright 2017, Wiley-VCH.

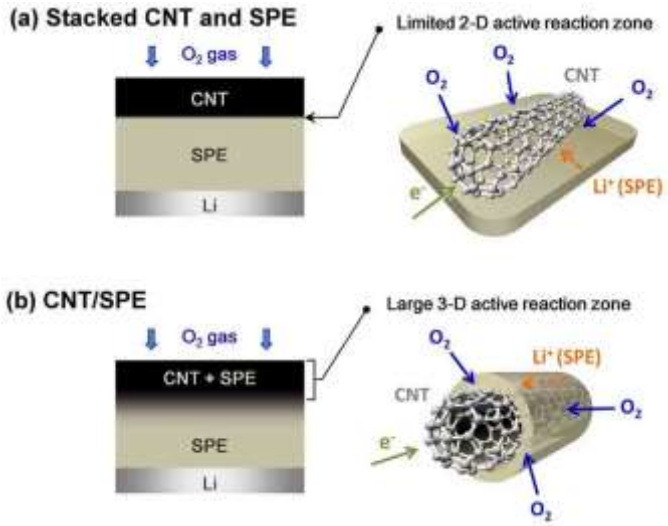

Fig. 12 Schematic illustrations of (a) limited 2D active reaction zone in conventional CNT and SPE sandwiched structure and (b) enlarged 3D active reaction zone in 3D CNT/SPE architecture. Reprinted with permission from ref. 125, copyright 2014, Nature Publishing Group.

In addition to the limited interfacial reaction areas, the high interface resistance between the polymer electrolyte and Li_2O_2 is another challenge for LABs, resulting in a low energy efficiency and even the instabilities of the electrode and electrolyte. In conventional aprotic LABs, besides developing effective catalysts in the air electrode,[158] the use of redox mediator (RM) in the liquid electrolyte is regarded as an effective approach to improve the OER kinetics. During charge, RM is oxidized to RM^+ at the air electrode surface as:

$$RM \rightarrow RM^+ + e^- \quad (9)$$

which in turn oxidizes the solid Li_2O_2 into lithium ion and oxygen with a reverse reaction into the initial state:

$$Li_2O_2 + 2RM+ \rightarrow 2Li^+ + O_2 + 2RM \quad (10)$$

Different kinds of RMs have been developed in aprotic LABs,[130,159–163] while their applications in polymer electrolytes are still limited. Zhou *et al.* reported a stable RM-decorated GPE, through which the terminal charge voltages decreased due to the improved interface between the electrolyte and the solid product.[164] The similar approach was reported by Li *et al.*, in which the RM-decorated GPE resulted in 100 cycles at a fixed capacity of 1000 mAh g^{-1}, which is nearly twice the cycle number of the pristine GPE (55 cycles).[116]

Although the results from the RM-decorated GPE are promising, it is worth noting that the lithium metal anode may be attacked by a RM, limiting the cycle life.[160,161] In addition, the use of RM is limited in the GPEs with the existence of liquid electrolytes, while for the other polymer electrolytes such as SPEs and CPEs, how to solve the high interfacial resistance between the solid Li_2O_2 and the electrolyte remains challenging.

These above-mentioned issues are crucial for ZABs and LABs with electrolyte membranes. In flexible MABs, besides the internal electrode-electrolyte interface issues, the external forces can also cause the damage of the interfaces due to the different elastic modulus of the electrodes and the electrolyte membrane. Hence, when developing electrolyte membranes, the maintenance of stable electrode-electrolyte interfaces, especially under bending and even twisting conditions, is crucial for the stable operation.

5. Air electrode

The air electrode provides the reaction places for both ORR and OER and is regarded as a significant component in MABs. As illustrated in **Fig. 2a**, the ORR in ZABs occurs at the three-phase boundaries so that an optimal hydrophilicity is crucial, which requires hydrophilic microchannels for providing access to the liquid electrolyte and hydrophobic counterparts to prevent electrolyte leakage and facilitate gaseous oxygen diffusion.[18] To this end, a typical air electrode consists of a substrate and a catalyst layer. The substrate provides a physical and conductive support for the catalysts and a pathway for oxygen diffusion during discharge and charge. The basic requirements include a high electrical conductivity, high mechanically stability, and 3D porous structure. The catalyst layer is composed of bi-functional catalysts, carbon conductive matrix, and binders for ORR and OER processes.[7,44,45,158] The similar structure has also been applied in the air electrode of LABs, although the hydrophilicity seems unimportant since most organic solvents can easily flood the whole electrode to form two-phase boundaries (**Fig. 2b**).[20] To be employed in flexible MABs, unfortunately, the conventional electrode with a rigid substrate such as carbon paper become not applicable; and the one with a high flexibility is essential. The catalyst materials applied in ZABs and LABs have been summarized in a number of reviews.[7,36,44,158] So this section focuses on different kinds of flexible substrates that have already been used or demonstrated the potential to be used in flexible MABs. The carbon-based substrates, including the ones made of woven carbon fibre and carbon nanomaterials, are first summarized. Then, metal substrates, due to their high stabilities and good fatigue resistances, are reviewed. Moreover, some novel flexible substrates that have promising applications are also introduced.

5.1 Carbon substrate

Different from rigid carbon paper, carbon cloth is made of woven carbon fibers (**Fig. 13a**)[165] and more mechanically flexible. Fu *et al.* coated the perovskite lanthanum nickel oxide/nitrogen-doped carbon nanotubes ($LaNiO_3$/NCNT) catalyst on a flexible carbon cloth and used as the air electrode in a flexible ZABs.[71] Besides $LaNiO_3$/NCNT, cobalt oxide (Co_3O_4) nanoparticles were loaded on a carbon cloth to form an air electrode.[77] In addition to coating catalysts and binders onto the surface of carbon cloth, directly decorating catalysts on the carbon cloth surface for a free-standing, binder-free, and integrated air electrode has been developed for flexible ZABs and LABs.[79,80,84–86,88,91,132,166] For instance, Yu *et al.* developed Nitrogen-doped Co_3O_4 nanowires on a carbon cloth as an additive-free air electrode for flexible solid-state ZABs. The catalytic activity is promoted by the nitrogen dopant through enhanced electronic conductivity, increased oxygen adsorption strength, and improved reaction kinetics. As a result, the ZAB based on the

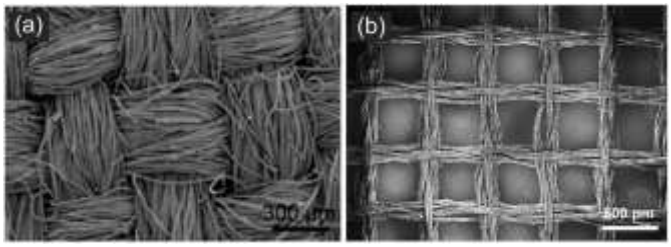

Fig. 13 SEM image of (a) carbon cloth. Reproduced with permission from ref. 165, copyright 2014, The Royal Society of Chemistry. (b) carbon mesh. Reproduced with permission from ref. 167, copyright 2016, Elsevier.

optimized electrode exhibited a high volumetric capacity of 98.1 mAh cm^{-3} and outstanding flexibility.[79] Zhang *et al.* grew TiO_2 nanowire arrays onto the carbon cloth and applied in a flexible LAB, which showed superior electrochemical performances even under stringent bending and twisting conditions.[85] Meng *et al.* in-situ coupled the strung Co_4N and intertwined N–C fibers on the carbon cloth to obtain a free-standing and highly flexible bi-functional air electrode. Originating from the synergistic effect of Co_4N and Co–N–C and the stable 3D interconnected conductive network structure, the electrode exhibited high electrocatalytic activities and stabilities for both OER and ORR, enabling excellent performance in cable-type flexible ZABs and LABs.[91]

Besides commercial carbon cloth, other substrates made of carbon fibres have also been developed. Lim *et al.* reported a substrate of carbonaceous meshes (CMs), which were formed by the heat treatment of waste silk fabric, as shown in **Fig. 13b**.[167] This substrate not only has a hierarchical pore structure, but also possesses favourable mechanical properties and chemical stabilities, including a high electrical conductivity of ~150 S cm^{-1}, a tensile strength of 34.1±5.2 MPa, and an elastic modulus of 4.03±0.7 GPa. When applied in a LAB, the all-carbon-based CM electrode delivered a high energy density of ~2600 Wh $kg_{electrode}^{-1}$ along with stable cycling.

In addition to carbon cloth and mesh, different kinds of carbon nanomaterials have also been used to fabricate carbon substrates. A free-standing film made of CNTs (also known as buckypaper) has been developed without the employment of binders, preventing the surface loss (**Figs. 14a-b**).[168] In addition, the interconnected CNTs form a porous structure with proper pore spaces,[169] facilitating the transport of species. With these advantages, the buckypaper has been applied as the air electrode in ZABs and LABs.[170–173] For instance, a buckypaper electrode made of MWCNTs in a LAB delivered a high specific capacity of 34,600 mAh g_{CNT}^{-1} and 50 cycles at a fixed capacity of 1,000 mAh g^{-1}.[174] Besides using alone, the buckypaper can also be used a platform for the catalyst decoration to form an integrated electrode. Lim *et al.* decorated Pt nanoparticles and obtained stable performance for over 130 cycles at a high current rate of 2 A g^{-1} in a LAB.[175] Tan *et al.* used RuO_2 nanoparticles to decorate the buckypaper and achieved an energy efficiency up to 70%.[168] Attributed to its superior mechanical strength and flexibility (tensile strength: 11.53 MPa; elastic modulus: 2.24 GPa)[173], the buckypaper is also a promising electrode material for flexible MABs.[87,90,92]

Carbon nanofibers (CNFs) have also been used to fabricate a free-standing and binder-free film, as shown in **Figs. 14c-d**.[74] Through electrospinning and carbonization, a flexible CNF film with designed pore structure and a high electrical conductivity and mechanical stability (tensile strength: 1.89 MPa; elastic modulus: 0.31 GPa) can be obtained.[74] Similar to the CNT film, the CNF film can also be the platform for catalyst decoration.[176–178] Xue *et al.* fabricated a 3D hierarchical porous hybrid film composed of $NiCo_2O_4$ nanoparticle-decorated mesoporous nitrogen-doped CNF. When served directly in LABs, benefiting from the structural and material superiority, it exhibited a high specific capacity of 5304 mAh $g_{electrode}^{-1}$, excellent rate capability, and outstanding cycling stability of nearly 100 cycles.[179] Liu *et al.* developed flexible nanoporous CNF films as the air electrodes for ZABs.[74] In a conventional battery, it exhibited excellent electrochemical performance, including a high open-circuit voltage of 1.48 V, a maximum power density of 185 mW cm^{-2}, a round-trip efficiency of 62%, and a high stability with the voltage gap increased to only 0.13 V after 500 cycles. More importantly, a flexible ZAB with this

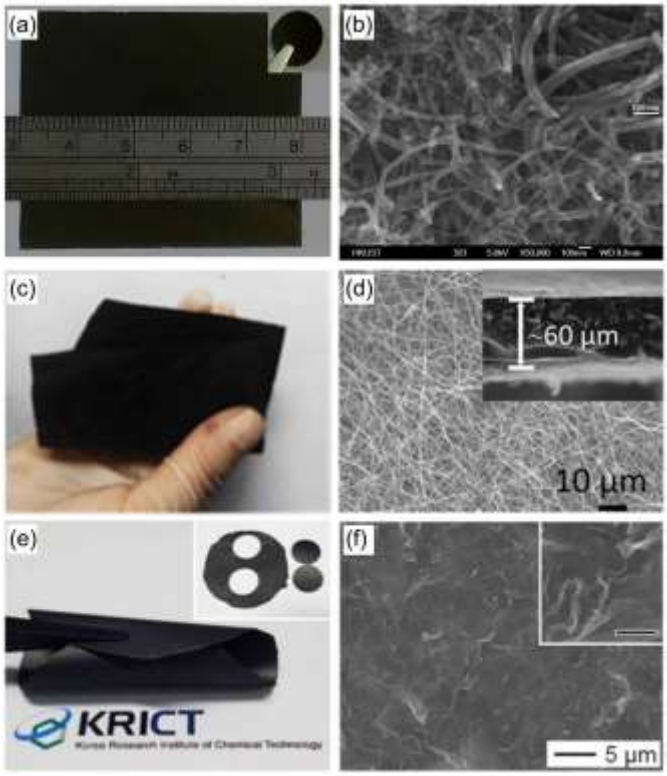

Fig. 14 Free-standing electrode made of carbon nanomaterials: (a-b) CNT paper: (a) photograph of the CNT paper, inset shows a disc-like electrode with a diameter of 8 mm; (b) SEM image of the top view, inset shows the image with a higher magnification. Reproduced with permission from ref. 168, copyright 2015, The Royal Society of Chemistry. (c-d) CNF paper: (c) photograph of the flexible carbon nanofiber paper; (d) SEM image, inset shows the thickness of the paper. Reproduced with permission from ref. 74, copyright 2016, Wiley-VCH. (e-f) GNP/GO paper: (e) Photograph of the as-prepared GNP/GO paper with a diameter of ~37 mm, demonstrating its flexibility, inset shows the photograph of the GNP/GO paper (cut using a hole punch with a diameter of 12 mm); (f) SEM image of the top view, inset shows the image with a higher magnification (scale bar: 1 µm). Reproduced with permission from ref. 180, copyright 2015, Elsevier.

electrode displayed an excellent mechanical and cycling stability with low overpotentials as well as a long cycle life even under repeated bending conditions.

Graphene has great potential to be used for energy storage systems due to its excellent electrical conductivity, extremely high theoretical surface area (2630 m^2 g^{-1}),[181,182] and high graphitization degree, which makes it much more stable than other carbon materials. In addition, graphene has high mechanical strength as well as high flexibility, enabling the individual sheets to be arranged into free-standing paper-like structures without any conducting additives and binder.[183] Cetinkaya *et al.* reported a free-standing and flexible graphene oxide (GO) paper, which showed good flexibility and could be directly used as the air electrode in LABs.[184] Kang *et al.* fabricated highly flexible and porous free-standing graphene papers, which were composed of graphene nanoplatelet (GNP) and GO.[185] It reached a maximum conductivity of 176 S cm^{-1} with a thickness of 10 µm and a high surface area of 278.9 m^2 g^{-1}. As shown in **Fig. 14e**, the GNP/GO paper is free-standing and had sufficient flexibility to be bent, rolled, or even folded, and can be easily cut using a hole punch. The SEM image (**Fig. 14f**)

demonstrates that the GNP/GO paper has a wrinkled and disordered structure throughout the paper, which could be attributed to the partial re-aggregation of the GNPs under the holding effect of the GOs during the drying process. When applied in a LAB, the GNP/GO paper electrode showed reversible cycles with a relatively high energy efficiency of 87%.[180] Besides using GO along, a free standing α-MnO_2/GO composite paper was fabricated by Ozcan *et al.*, which showed the improved electrochemical performance in a LAB.[186]

5.2 Metal substrate

Although carbon substrates have advantages of lightweight, easy fabrication, and low cost, the carbon corrosion is a challenging issue during the battery operation. In ZABs, when encountering highly oxidative electrochemical potentials during charge, the carbon may be readily corroded,[187,188] aggravating aggregation/sintering or even leaching of catalysts, severely reducing the performance.[18] In LABs, carbon materials can chemically react with the oxidative products (e.g., LiO_2, Li_2O_2)[189,190] or electrochemically decompose at high charge potentials,[191] forming irreversible side products covering the active sites at the air electrode, leading to the electrode passivation and capacity fading during cycling.[192] Consequently, preventing the corrosion of carbon substrates is important for long-term operation. One approach is to use carbon materials with a high graphitization degree such as CNT and graphene. Another approach is to choose metal-based substrates as the alternatives, such as nickel form, stainless-steel (SS) mesh, and titanium mesh. They provide higher electrical conductivities and electrochemically oxidative stabilities and thus have been applied in both ZABs and LABs.[193–200] To be applied in the flexible metal-air batteries, a high flexibility with good structural robustness is also crucial.

Chen *et al.* developed a 3D air electrode for ZABs through directly growing Co_3O_4 nanowire as the active material onto the surface of SS mesh.[201] Non-conductive ancillary binding materials are removed from the electrode, avoiding the decomposition of binders and enhancing the electrical property and the electrochemical stability. In addition, the mechanical flexibility of the SS mesh allows bending of the electrode, showing the significant potential for flexible device applications. Based on the SS mesh, they also designed a hair-like catalyst array containing a nanoassembly of two-dimensional (2D) mesoporous Co_3O_4 nanopetals in a one-dimensional (1D) nitrogen-doped MWCNT (NCNT), as shown in **Fig. 15a**.[72] This hair-like structure of the Co_3O_4-NCNT nanoassembly can provide intimate interfacial contact between Co_3O_4 and NCNT, favoring a low-resistance pathway for a high flux of charge transfer during ORR and OER. Additionally, the decoration of Co_3O_4 nanopetals changes the wettability of the air electrode and facilitates the diffusion of oxygen inside the electrode during the ORR. Moreover, the air electrode exhibits a superior flexibility, which could be twisted even at a torsion angle of 360° (**Figs. 15b-c**). A flexible ZAB was built with this electrode, and the discharge and charge potentials of the rolled-up battery remained virtually unchanged at different angles, indicating a robust mechanical integrity of the SS-based electrode.

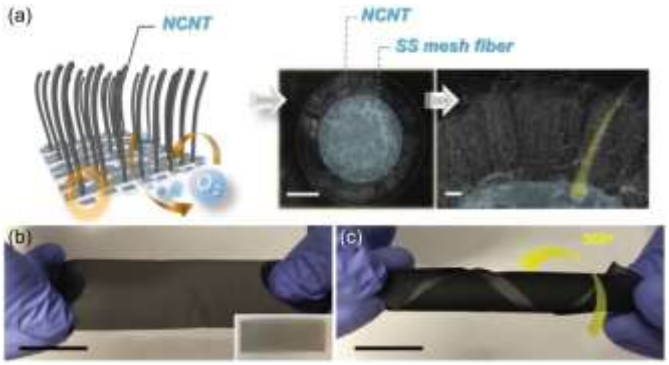

Fig. 15 (a) Illustration and cross-sectional SEM images of vertically aligned NCNT framework directly grown on the surface of every individual SS mesh fiber. (b-c) Digital photos of the Co_3O_4-NCNT/SS electrode (b) without and (c) with twisting the electrode to 360°. The scale bar is 2 cm. Reproduced with permission from ref. 72, copyright 2016, Wiley-VCH.

Although other metal substrates also demonstrate good flexibilities (e.g., nickel mesh, titanium mesh), their applications in flexible MABs are still rarely reported. It is worth noting that even though metals have improved electrochemical stabilities than those of carbons, their long-term stabilities still require great attention.[202] In addition, during bending, twisting, and even stretching processes, the fatigue of metal substrates should be carefully addressed. Moreover, compared with carbon materials, the larger densities of metal substrates (e.g., nickel, steel) inevitably lower the practical specific capacities and energy densities of the whole battery.[203] These issues should be taken into consideration when developing metal-based air electrodes.

5.3 Others

Besides carbon- and metal-based substrates, some novel types of flexible electrodes have also been developed. Clark *et al.* developed a paper-based ZAB through screen-printing a zinc composite anode on one side of a paper sheet and a cathode on the other side.[204] However, the paper/electrolyte combination has a limited ability to take up anode oxidation products before suffering a reduction in ionic mobility. Based on the commonly used paper, Zhang *et al.* developed a paper-ink electrode through simply drawing ink on the paper. Compared with conventional carbon electrode materials, it is cost effective and synthesis facile. In addition, the active material could homogenously adsorb onto the paper skeleton, ensuring the formation of a free-standing structure. With this novel electrode as both air electrode and current collector, a foldable LAB has been achieved (**Fig. 5a**).[82]

Lin *et al.* proposed a novel free-standing air electrode by using industrially wearable and highly conductive metal wire/cotton fibre yarns.[94] As schematically shown in **Fig. 16a**, by dyeing with RuO_2-coated nitrogen-doped CNTs (RuO_2/N-CNTs) ink, a conductive and flexible air electrode is synthesized (**Fig. 16b**). Compared with a conventional air electrode, it has following advantages: First, the inexpensive, flexible, lightweight cotton fibre bending with the metal wire serves as a substrate of active material and the current collector, making the battery foldable and bendable. Second, the structure of multiple microfibrils bundled in the cotton fibre allows to absorb a large amount of liquid electrolyte and effectively avoid the leakage. Third, printing and dyeing properties of the cotton yarn make it easy to load a variety of functional materials. When assembled into a cable-type LAB, a discharge capacity of 1981 mAh g_{carbon}^{-1} was delivered. Besides, the battery could work for 100 cycles (over 600 h) without obvious degradation even under bending condition, demonstrating outstanding flexibility and stability.

One-dimensional conducting nanomaterials, such as metallic nanowires (NWs), are good candidates for a conductive scaffold.[205] They can form a highly porous and conductive framework when randomly percolated, and serve as the catalyst for efficient formation and decomposition of the discharge products in

MABs.[206–209] Jung *et al.* designed a porous and carbon-free conducting nanopaper (CNp), which is composed of conducting NWs bound by a chitin binder as schematically shown in **Fig. 16c**.[210] Chitin is renowned for its chemical inertness to most organic solvents and tendency to form crystalline supramolecules, while employing a low amount (<1 wt%) of chitin binder to connect the conductive skeleton can maximize the pores and active sites for reactions (**Fig. 16d**). The structural integrity of the CNp is robust enough that could be possible to cut the self-standing mat readily into various geometries without structural collapse. When applied in a LAB, the carbon-free CNp enabled more than 190 cycles (over 950 h), which was more stable compared to CNFs and CNps bound by other binders.

For the further development of air electrodes, a novel integrated design is expected which is directly growing nanostructured catalysts on the substrates. Without additional carbon matrix and binders, a high accessibility of active sites and a low interfacial contact resistance can be provided. In addition, the integrated air electrodes are directly synthesized without complex preparation processes, benefiting the large-scale fabrication.[18] When choosing the substrate, the one with a high electrical conductivity and chemical/electrochemical stabilities, as well as mechanical robustness is demanded. In addition, the density should be taken into account for a high specific capacity and energy density.[211] When developing the catalyst, searching for inexpensive alternatives to noble metals, especially with bi-functional catalytic activities, should be the ultimate target.[7] To determine the real electrochemical activity, apart from using voltage profiles, more quantitative methods are required.[39] For example, early studies of catalysts in LABs were later proven to catalyze the decomposition of carbonate-based electrolytes rather than the desired formation and decomposition of Li_2O_2.[212] Even with a relatively stable solvent (i.e., TEGDME), Peng *et al.* used differential electrochemical mass spectrometry (DEMS) to monitor the charge process and demonstrated that the noble metal catalysts (e.g., Pd, Ru) did not work according to the desired electrochemistry, but decreased O_2 recovery efficiency and increased CO_2 evolution during charge, impairing the reversibility.[213] Hence, the electrochemical performance evaluation of the air electrode should be carried out in a comprehensive scope.[214] Moreover, in flexible ZABs and MABs, an electrolyte membrane is applied instead of the liquid electrolyte so that the electrolyte-air electrode interfaces are greatly changed as introduced in Section 4.3.2. Therefore, tremendous research efforts are needed to developing novel air electrodes associated with effective substrates and catalysts.[113]

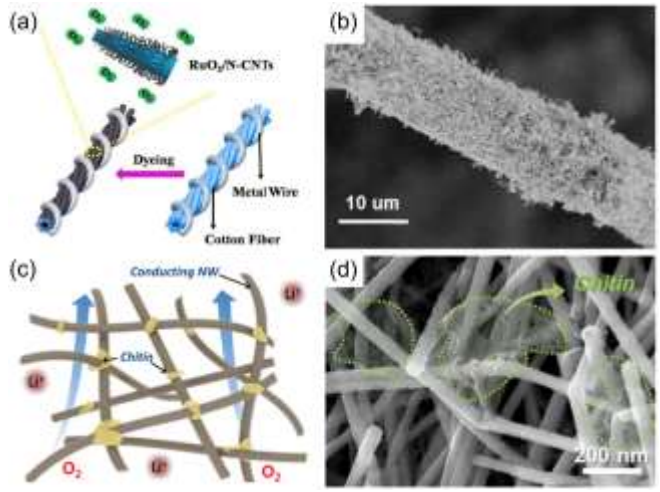

Fig. 16 Some novel electrode materials: (a) Schematic illustration and (b) SEM image of the metal/cotton yarn electrode. Reproduced with permission from ref. 94, copyright 2017, The Royal Society of Chemistry. (c) Schematic structure and (d) SEM image of the carbon-free conducting nanopaper. Reproduced with permission from ref. 210, copyright 2017, American Chemical Society.

6. Operation management

Most ZABs are tested in the ambient air atmosphere. In contrast, LABs are usually tested in the pure oxygen atmosphere due to their high sensitivity to the moisture. While for practical applications of flexible MABs, the operation in ambient air is essential for achieving high capacities and energy densities. Therefore, understanding the detrimental effects of carbon dioxide and moisture on ZABs and LABs and corresponding solutions are significant. Besides, the temperature in different seasons and regions can vary significantly. The effects of temperature on the battery performance are also important.

6.1 Gas contaminations

6.1.1 Effects of carbon dioxide on Zn-air batteries

When operating ZABs in ambient air, the carbon dioxide (CO_2) can easily react with alkaline electrolytes to form carbonates. The effect of CO_2 on the electrochemical performance has been investigated in conventional batteries. Results showed that the formation of carbonates not only reduces the electrolyte conductivity, but also clogs pores and decreases the active surfaces in the air electrode when crystallization of carbonates occurs.[15] Hence, the existence of CO_2 in ambient air is a predominant threat to the operation of alkaline ZABs.[20]

The effects of CO_2 poisoning on the electrochemical performance of a ZAB with a solid-state electrolyte membrane QAFC has been investigated by Chen *et al.*[73] The galvanostatic discharge and charge of the battery were performed under oxygen and the oxygen containing 20,000 ppm CO_2 (~50 times higher than that of air), respectively (**Fig. 17a**). Compared to the pure O_2 condition, the initial higher polarization in the presence of CO_2 is likely related to increased ion (OH^- and CO_3^{2-}) transport resistances of the membrane, correlating with the result that the membrane with the anion type of CO_3^{2-} has a smaller conductivity than that of the membrane with the anion type of OH^-. The polarization was progressively smaller for the first 420 minutes, while after that only a slightly higher polarization was observed. The results indicated the reduction in the residual carbonate content in the QAFC membrane, leading to the similar battery performance between the case of pure O_2 and CO_2/O_2 mixture after 420 min. This may be caused by a high level of in situ ''self-purging'' process occurring at the air electrode, where OH^- anions are continuously generated through ORR under high current densities.[215] Additionally, the increased pH environment was beneficial for the reaction kinetics, improving the battery performance. Hence, the charge-transfer resistance of the battery in the present of CO_2 decreased after 420 min (i.e., 2010th min) compared to that at the initial stage (i.e., 90th min), as revealed in the electrochemical impedance spectroscopy (EIS) shown in **Fig. 17b**.

For flexible ZABs, although promising results have been demonstrated in ambient air, the investigation of CO_2 effect on the long-term stability is still absent. In ZABs for stationary energy storages (e.g., power plan, EVs), CO_2 can be effectively removed by

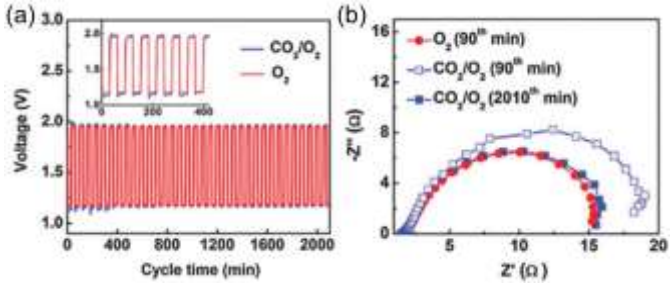

Fig. 17 (a) Galvanostatic charge and discharge cycling of the battery using pure oxygen and 20,000 ppm CO_2 contaminated gas reactants, respectively, at a current density of 250 mA g^{-1} with a 60 min per cycle. Inset shows an extended view of the first 420 min. (b) Corresponding Nyquist plots of the impedance of the battery at designated time segments. Reproduced with permission from ref. 73, copyright 2016, The Royal Society of Chemistry.

passing the inlet air through a ''scrubber'' of inexpensive hydroxides (e.g., soda lime and $Ca(OH)_2$) or amines (e.g. mono-ethanolamine).[216,217] While for flexible ZABs which are used for electronic devices, this method seems inapplicable. Developing an oxygen selective membrane with a high selectivity may be helpful for the robustness operation of ZABs in ambient air, but more intensive studies are needed.

6.1.2 Effects of carbon dioxide and moisture on Li-air batteries

In comparison with ZABs, the operation of LABs in ambient air faces more challenges. First of all, the common ambient air is a gas mixture containing oxygen with a partial pressure of only 0.21 atm,[32] which could greatly lower the electrochemical performance since most of the reported battery performance was obtained in a pure oxygen environment with a pressure equal to or greater than 1.0 atm.[218–220] Besides, the water moisture in ambient air can contaminate the lithium electrode, forming side products covering the lithium surface and increasing the lithium ion transport resistance, resulting in a waste of lithium and high overpotentials.[221–224] Moreover, both CO_2 and H_2O can participate in the electrochemical/chemical reaction occurring in the air electrode to form side products like Li_2CO_3 and LiOH with poor rechargeability.[225,226] They accumulate on the electrode surface during cycling, decreasing the active sites and leading to rapid degradation in performance or even failure in operation.[227]

To protect the lithium electrode from moisture, a ceramic lithium conducting plate has been added in between the cathode and the anode.[228] However, the fragile property hinders its wide application, especially in flexible batteries. To this end, Choi *et al.* introduced a poreless polyurethane (PU) membrane.[229] The poreless character of the PU separator prevents water and oxygen from penetrating and gaining access to the lithium metal surface, while lithium ion diffusion is facilitated by high electrolyte uptake through the interchain space. Due to the enhanced stability at the lithium electrode-electrolyte interface, the battery exhibited more than 200 cycles at a fixed capacity of 600 mAh g^{-1}. Wu *et al.* developed a super-hydrophobic H_2O-preventing quasi-solid electrolyte (SHQSE) membrane through coating super-hydrophobic silicon dioxide (SiO_2) and polyisobutylene (PIB) binder onto the non-woven fabrics.[230] The prepared SHQSE membrane with the thickness of 30 μm can be bent at the large angle of 180° without any crack, showing a good flexibility. It also exhibited a large H_2O contact angle of over 150°, indicating the super-hydrophobic surface. When incorporated with a hydrophobic ionic liquid-based electrolyte membrane, a LAB could achieve a long cycle life in a humid atmosphere with the RH of 45%. For flexible LABs, Zhang *et al.* fabricated a PVDF-HFP based GPE with not only an excellent bendability (**Fig. 18a**) but also a good hydrophobicity as displayed in **Fig. 18b**,[93] which might effectively prevent the penetration of moisture into the lithium anode. As demonstrated in **Fig. 18c**, the lithium rod with GPE is stable in water. In contrast, violent reaction happened immediately without the GPE protection. As a result, the cable-type flexible LAB with this GPE could still work even partially immersed in water (**Fig. 18d**),[93,95] demonstrating the effective protection of the lithium electrode.

Even though the lithium electrode is well protected, the accumulation of irreversible side products (e.g., Li_2CO_3, LiOH) in the air electrode during air-operation is still a critical issue. Peng *et al.* investigated the electrochemical performance of a sandwich-type flexible LAB in ambient air with a RH of ~5% at room temperature.[87] They found that in addition to the formation of reversible Li_2O_2 as the main product, LiOH and Li_2CO_3 were also detected with increasing cycles. The accumulation of these side products during long-period cycling was associated with the increasing charge overpotentials. When operating at a higher RH of ~20%, the cycle life degraded remarkably from over 180 cycles to less than 70 cycles. Similar results have also been reported for a cable-type flexible LAB tested in ambient air with a RH of ~5%, in which LiOH and Li_2CO_3 were detected after five cycles.[92] It should be noted that the actual ambient RH could be between 50% and 70%, or even about 90% in tropical or sub-tropical areas. Consequently, the effect of actual RH on the battery performance and durability may be underestimated from the above-mentioned studies. Hence, effective approaches are needed to enable the stable electrochemical performance. One solution is to use an oxygen selective membrane as suggested for ZABs. However, the substantial thickness and limited surface area of reported membranes for LABs caused an increase in the oxygen transport resistance, leading to a sacrifice in the performance.[231–235] Hence, developing an oxygen selective membrane that with a high oxygen permeability and selectively is still challenging.[236,237] In addition, finding proper catalysts that can efficiently promote the decomposition of side products is another strategy. Zhou *et al.* showed that Ru nanoparticles supported on Super P can help the

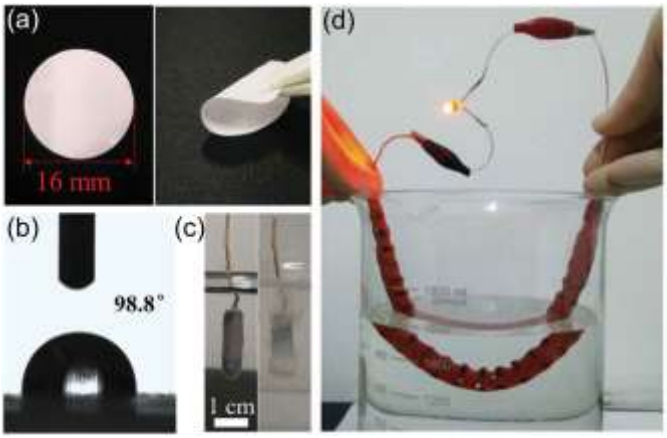

Fig. 18 Optical photographs of (a) the fabricated GPE at flat and bend conditions, (b) water contact angle, (c) Li rod immersed in water with (left) and without (right) the protection of the GPE membrane, (d) A cable-type flexible LAB powered a commercial red LED immersed in water. Reproduced with permission from ref. 93, copyright 2016, Wiley-VCH.

decomposition of LiOH at a low charge overpotential (0.21 V).[238] They further integrated a hydrophobic ionic liquid-based electrolyte and an air electrode composed of MnO_2 and RuO_2 supported on Super P, which enabled a LAB to be sustained in a humid atmosphere (RH=51%) with a high discharge voltage of 2.94 V and the low charge voltage of 3.34 V for 218 cycles.[239] In addition to RuO_2,[240,241] it is found that the Au-decorated δ-MnO_2 could also catalyze the decomposition of LiOH to some extent.[227] Focused on CO_2, Li *et al.* developed a Li-CO_2:O_2 (2:1) battery in which Li_2CO_3 is the main product that can discharge and charge reversibly.[242] Moreover, rechargeable Li-CO_2 batteries have attracted research interests recently,[243–245] and the reversibility could be achieved through CNT,[244,246] graphene,[247] and Ru nanoparticle-deposited carbon,[248] and the decomposition mechanism has also been investigated.[249,250] Besides carbons, NiO was reported to be an effective catalyst for Li_2CO_3 decomposition [251–253] and a ultrafine iridium-decorated boron carbide (Ir/B_4C) nanocomposite could even decompose Li_2CO_3 with an efficiency close to 100% at a voltage below 4.37 V.[254] These catalysts may be incorporated into the air electrode to address the side products for enabling the stable operation of flexible LABs in ambient air.

6.2 Temperature effects

In most reported flexible metal-air batteries, electrochemical performance evaluation was conducted at room temperature (i.e., 25 °C).[70] However, the temperature variation in different seasons and in different regions could be significant (e.g. -30 °C in winter in some areas and 40 °C in summer in some parts of the world). For wearable devices (e.g., smart watch, wristbands), a direct contact of the human body may increase the operating temperature to a value higher than 30 °C. Besides, the heat generation from chips in electronic devices may further increase the operating temperature. For ZABs, on the one hand, higher temperatures would increase the solubility of carbonates and retard the precipitation;[20] on the other hand, the water loss may become severe, resulting in challenges for the GPEs. For LABs, the reaction mechanisms could be affected by temperature, leading to remarkably changed electrochemical performance.[255,256] Thus, effective thermal managements are critical for their electrochemical performance and durability. Cold start of flexible MABs in the sub-freezing environment is also critical for their application in cold regions. Therefore, apart from the undesired gasses in the formation of side products, the temperature effect is another factor that worth great attention in the future research and should be properly managed.

7. Conclusions and outlook

In conclusion, significant progress has been made in the development of flexible ZABs and LABs recently. Several configurations have been developed to enhance mechanical stabilities under different deformations while maintaining good electrochemical performance, including high discharge capacity, power density, energy efficiency, and long cycle life. However, many technical challenges still remain and breakthroughs in several critical areas are needed to develop a new generation of flexible metal-air batteries with dramatically enhanced performance and durability.

First, novel battery configurations are critical to meeting the demands for mechanical flexibility of batteries. The sandwich-type structure has been widely adopted, while a noteworthy design is the cable-type structure with extreme omnidirectional flexibility, which can be combined with textile technology to facilitate the emergence of wearable electronic devices. Even with this advance, to satisfy the requirements of bending, twisting, and even stretching, more innovative ideas are highly needed for the battery configuration. Different from the closed systems such as lithium-ion batteries and supercapacitors, a large open ratio (e.g., 25%) should be kept for the oxygen diffusion,[257] aggregating the design difficulties and the implantation in the flexible electronic devices. In addition, although some novel designs have been tried and some of them have demonstrated their potential for future development, few efforts have been made to optimize the structures and designs. A combined effort integrating mechanics and electrochemistry could be useful for understanding the electrochemical-mechanical behaviours of the flexible batteries and for subsequent design optimization.

Second, the energy density and cycle life of the current flexible MABs still need to be improved. For flexible ZABs, energy densities of 847.6 W h kg_{Zn}^{-1} and 5.7 Wh $L_{battery}^{-1}$ have been achieved in a sandwich-type battery[72] and a cable-type battery,[90] respectively, and a cycle life of over 500 h in ambient air has been demonstrated.[72] For flexible LABs, an energy density of 523.1 Wh kg^{-1} has been obtained in a bamboo slip-like battery,[95] and a long cycle life up to 356 cycles has been reported.[85] However, the uncertainty associated with the reported performance numbers of the flexible MABs is lack of a standard for normalization of the performance parameters. For example, the gravimetric (kg^{-1}) and volumetric (L^{-1}) capacity or energy density should be normalized by mass or the volume of the entire battery rather than by the catalyst loading or the superficial electrode area. In addition, the energy density and cycle life are usually measured under the initial conditions without any deformations, while a clear definition of "standard testing procedures" is yet to be defined to take into consideration of deformation under service conditions. Hence, more comprehensive mechanical testing should be used to evaluate the flexibility of batteries or battery components, including bending and/or twisting to different angles and testing the stabilities under long bending/stretching cycles. It is important to establish a standard benchmarking procedure and parameters for making a fair comparison of this technology with other energy storage systems. Also, a more systematically evaluation is necessary that includes both mechanical flexibility and the electrochemical performance.

Third, the fabrication of flexible MABs requires a flexible current collector, flexible electrode materials, a flexible electrolyte membrane, and a flexible encapsulating material. To maintain stable electrochemical performance under deformation, each component must be carefully designed.

i) For the metal electrode, besides addressing the conventional issues such as dendrite formation and surface passivation, continuous bending and stretching of the metallic plate may cause mechanical or electrical failure of the electrode. In addition, the metal plate can hardly satisfy the requirements of stretching. To this end, modifications such as changing the electrode shape (e.g., spring-like for stretchable), using a free-standing composite flexible electrode, and forming a fatigue-resistant electrode should be employed.

ii) For the electrolyte membrane, the gel polymer electrolytes demonstrate a number of advantages including high ionic conductivities and flexibilities, while the existence of liquid electrolytes limits their long-term application in the open systems due to the possible evaporation. Especially for LABs, the flammable aprotic electrolytes also bring safety problems. The solid and composite polymer electrolytes seem to be a remedy, while they usually suffer from low ionic conductivity.

Besides, the electrolyte-electrode interfacial properties are crucial. At the air electrode-electrolyte interface, the dendrite formation and/or surface passivation will affect the reversibility of the metal electrode; while at the electrolyte-air electrode interface, the solid-state electrolyte membrane results in the limited reaction boundaries; both of which are detrimental to the electrochemical performance. Moreover, the external force during the bending or twisting process may damage the interfaces due to the different elastic modulus of electrolyte and electrodes. These issues are worth great attention in future developments of electrolyte membranes.

iii) For the flexible air electrode, different kinds of substrates have been proposed, and a variety of bi-functional catalysts have been developed. An integrated electrode with a high electrical conductivity, high chemical/electrochemical stabilities, high catalytic activities, as well as good mechanical robustness is highly demanded. Importantly, more quantitative methods are required to evaluate the electrochemical performance in a comprehensive scope.

Besides these main components, other parts (such as the flexible current collector and encapsulating materials) are also important to the battery stability and performance, and intensive investigations are needed.

Fourth, the operation management is highly important for the practical application. As a half-open system, the contaminations of carbon dioxide and moisture should be carefully studied and addressed, especially for LABs. Using an oxygen selective membrane is an effective approach to address the contamination issues, but the one with a high selectivity and flux is still challenging. Besides, the temperature variation in different seasons and regions could be significant. In wearable electronic devices (e.g., smart wristbands), the operating temperature may be fluctuated due to the contact of the human body, affecting the electrochemical performance. Hence, detailed investigations and corresponding thermal managements are needed.

In summary, although flexible MABs have promising potential among flexible energy storage systems, the research and development of these devices are still in the early stage and many technical hurdles are remained. Among them, the most critical one is the lack of fundamental understanding of the coupled transport and electrochemical process associated with the battery operation under external mechanical forces. It usually involves a series of elementary charge and mass transfer processes along the surfaces, across the interfaces, and through the bulk of some phases in a complex electrode, leading to difficulties in determination of the rate-limiting step of the overall process. To unreal the detailed mechanism and identify the rate-limiting step, it is necessary to track the evolution in the structure, composition, and morphology of electrodes as well as the charge and mass transport characteristics during the battery operation and deformation. It is necessary to use in situ/operando characterization tools to probe the structure, composition, and morphology of electrodes under operating conditions to correlate these microscopic features with the electrochemical performance. In addition, multi-scale modeling and simulation are imperative in gaining important insights into the mechanism of these complex phenomena, which is vital to achieving rational designs of better materials and novel battery configurations for high-performance flexible MABs.[258] With tremendous efforts, flexible MABs have potential to be the promising power sources for flexible electronic systems. The insights gained from innovative investigations may also benefit other flexible energy storage systems such as flexible sodium batteries and supercapacitors.

Acknowledgements

M. NI thanks the funding support from The Hong Kong Polytechnic University (G-YBJN and G-YW2D), the Environment Conservation Fund (ECF 54/2015) and a fund from RISUD (1-ZVEA).

References

1 K. Xie and B. Wei, *Adv. Mater.*, 2014, **26**, 3592.
2 B. D. Gates, *Science*, 2009, **323**, 1566.
3 S. Bauer, *Nat Mater*, 2013, **12**, 871.
4 C. Xie, J. Liu, T.-M. Fu, X. Dai, W. Zhou and C. M. Lieber, *Nat Mater*, 2015, **14**, 1286.
5 H. Lee, T. K. Choi, Y. B. Lee, H. R. Cho, R. Ghaffari, L. Wang, H. J. Choi, T. D. Chung, N. Lu, T. Hyeon, S. H. Choi and D.-H. Kim, *Nat Nano*, 2016, **11**, 566.
6 X. Wang, X. Lu, B. Liu, D. Chen, Y. Tong and G. Shen, *Adv. Mater.*, 2014, **26**, 4763.
7 Z.-L. Wang, D. Xu, J.-J. Xu and X.-B. Zhang, *Chem. Soc. Rev.*, 2014, **43**, 7746.
8 M.-S. Balogun, M. Yu, C. Li, T. Zhai, Y. Liu, X. Lu and Y. Tong, *J. Mater. Chem. A*, 2014, **2**, 10825.
9 L. Hu, H. Wu, F. La Mantia, Y. Yang and Y. Cui, *ACS Nano*, 2010, **4**, 5843.
10 M. S. Balogun, M. Yu, Y. Huang, C. Li, P. Fang, Y. Liu, X. Lu and Y. Tong, *Nano Energy*, 2015, **11**, 348.
11 M. S. Balogun, C. Li, Y. Zeng, M. Yu, Q. Wu, M. Wu, X. Lu and Y. Tong, *J. Power Sources*, 2014, **272**, 946.
12 M. S. Balogun, Z. Wu, Y. Luo, W. Qiu, X. Fan, B. Long, M. Huang, P. Liu and Y. Tong, *J. Power Sources*, 2016, **308**, 7.
13 P. Tan, M. Liu, Z. Shao and M. Ni, *Adv. Energy Mater.*, 2017, **7**, 1602674.
14 M. Winter and R. J. Brodd, *Chem. Rev.*, 2004, **104**, 4245.
15 J. S. Lee, S. T. Kim, R. Cao, N. S. Choi, M. Liu, K. T. Lee and J. Cho, *Adv. Energy Mater.*, 2011, **1**, 34.
16 B. Chen, D. Y. C. Leung, J. Xuan and H. Wang, *Appl. Energy*, 2017, **185**, 1303.
17 V. Caramia and B. Bozzini, *Mater. Renew. Sustain. Energy*, 2014, **3**, 28.
18 J. Fu, Z. P. Cano, M. G. Park, A. Yu, M. Fowler and Z. Chen, *Adv. Mater.*, 2017, **29**, 1604685.
19 G. Toussaint, P. Stevens, L. Akrour, R. Rouget and F. Fourgeot, *ECS Transactions*, 2010, **28**, 25.
20 Y. Li and H. Dai, *Chem. Soc. Rev.*, 2014, **43**, 5257.
21 M. Kar, T. J. Simons, M. Forsyth and D. R. MacFarlane, *Phys. Chem. Chem. Phys.*, 2014, **16**, 18658.
22 P. Sapkota and H. Kim, *J. Ind. Eng. Chem.*, 2009, **15**, 445.
23 J.-I. Jung, M. Risch, S. Park, M. G. Kim, G. Nam, H.-Y. Jeong, Y. Shao-Horn and J. Cho, *Energy Environ. Sci.*, 2016, **9**, 176.
24 P. Hartmann, C. L. Bender, M. Vračar, A. K. Dürr, A. Garsuch, J. Janek and P. Adelhelm, *Nat. Mater.*, 2013, **12**, 228.
25 H. Yadegari, Q. Sun and X. Sun, *Adv. Mater.*, 2016, **28**, 7065.
26 K. M. Abraham and Z. Jiang, *J. Electrochem. Soc.*, 1996, **143**, 1.
27 R. Black, B. Adams and L. F. Nazar, *Adv. Energy Mater.*, 2012, **2**, 801.
28 M. Park, H. Sun, H. Lee, J. Lee and J. Cho, *Adv. Energy Mater.*, 2012, **2**, 780.
29 S. S. Zhang, D. Foster and J. Read, *J. Power Sources*, 2010, **195**, 1235.
30 K. G. Gallagher, S. Goebel, T. Greszler, M. Mathias, W.

Oelerich, D. Eroglu and V. Srinivasan, *Energy Environ. Sci.*, 2014, **7**, 1555.
31 Y.-C. Lu, B. M. Gallant, D. G. Kwabi, J. R. Harding, R. R. Mitchell, M. S. Whittingham and Y. Shao-Horn, *Energy Environ. Sci.*, 2013, **6**, 750.
32 D. Geng, N. Ding, T. S. A. Hor, S. W. Chien, Z. Liu, D. Wuu, X. Sun and Y. Zong, *Adv. Energy Mater.*, 2016, **6**, 1502164.
33 R. Cao, J. S. Lee, M. Liu and J. Cho, *Adv. Energy Mater.*, 2012, **2**, 816.
34 M. A. Rahman, X. Wang and C. Wen, *J. Electrochem. Soc.* , 2013, **160**, A1759.
35 F. Cheng and J. Chen, *Chem. Soc. Rev.*, 2012, **41**, 2172.
36 D. U. Lee, P. Xu, Z. P. Cano, A. G. Kashkooli, M. G. Park and Z. Chen, *J. Mater. Chem. A*, 2016, **4**, 7107.
37 M. D. Radin and D. J. Siegel, eds. Z. Zhang and S. S. Zhang, Springer International Publishing, Cham, 2015, 511.
38 N. Imanishi, A. C. Luntz and P. Bruce, *The Lithium Air Battery*, Springer, New York, 2014.
39 D. Aurbach, B. D. McCloskey, L. F. Nazar and P. G. Bruce, *Nat. Energy*, 2016, **1**, 16128.
40 N. Feng, P. He and H. Zhou, *Adv. Energy Mater.*, 2016, **6**, 1502303.
41 F. Li and J. Chen, *Adv. Energy Mater.*, 2017, 1602934.
42 B. D. McCloskey, C. M. Burke, J. E. Nichols and S. E. Renfrew, *Chem. Commun.*, 2015, **51**, 12701.
43 X. Yao, Q. Dong, Q. Cheng and D. Wang, *Angew. Chemie Int. Ed.*, 2016, **55**, 11344.
44 N.-T. Suen, S.-F. Hung, Q. Quan, N. Zhang, Y.-J. Xu and H. M. Chen, *Chem. Soc. Rev.*, 2017, **46**, 337.
45 V. Neburchilov, H. Wang, J. J. Martin and W. Qu, *J. Power Sources*, 2010, **195**, 1271.
46 M. Balaish, A. Kraytsberg and Y. Ein-Eli, *Phys. Chem. Chem. Phys.*, 2014, **16**, 2801.
47 Z. Ma, X. Yuan, L. Li, Z.-F. Ma, D. P. Wilkinson, L. Zhang and J. Zhang, *Energy Environ. Sci.*, 2015, **8**, 2144.
48 Y. Li, X. Wang, S. Dong, X. Chen and G. Cui, *Adv. Energy Mater.*, 2016, **6**, 1.
49 K.-N. Jung, J. Kim, Y. Yamauchi, M.-S. Park, J.-W. Lee and J. H. Kim, *J. Mater. Chem. A*, 2016, **4**, 14050.
50 P. Pei, K. Wang and Z. Ma, *Appl. Energy*, 2014, **128**, 315.
51 J. Lu, L. Li, J.-B. Park, Y.-K. Sun, F. Wu and K. Amine, *Chem. Rev.*, 2014, **114**, 5611.
52 P. He, T. Zhang, J. Jiang and H. Zhou, *J. Phys. Chem. Lett.*, 2016, **7**, 1267.
53 M. Yu, W. Wang, C. Li, T. Zhai, X. Lu and Y. Tong, *NPG Asia Mater*, 2014, **6**, 129.
54 M.-S. Balogun, Y. Zeng, W. Qiu, Y. Luo, A. Onasanya, T. K. Olaniyi and Y. Tong, *J. Mater. Chem. A*, 2016, **4**, 9844.
55 M. S. Balogun, W. Qiu, F. Lyu, Y. Luo, H. Meng, J. Li, W. Mai, L. Mai and Y. Tong, *Nano Energy*, 2016, **26**, 446.
56 T. Zhai, X. Lu, F. Wang, H. Xia and Y. Tong, *Nanoscale Horiz.*, 2016, **1**, 109.
57 M. S. Balogun, Y. Luo, F. Lyu, F. Wang, H. Yang, H. Li, C. Liang, M. Huang, Y. Huang and Y. X. Tong, *ACS Appl. Mater. Interfaces*, 2016, **8**, 9733.
58 S. Xu, Y. Zhang, J. Cho, J. Lee, X. Huang, L. Jia, J. A. Fan, Y. Su, J. Su, H. Zhang, H. Cheng, B. Lu, C. Yu, C. Chuang, T. Kim, T. Song, K. Shigeta, S. Kang, C. Dagdeviren, I. Petrov, P. V Braun, Y. Huang, U. Paik and J. A. Rogers, *Nat. Commun.*, 2013, **4**, 1543.
59 Z. Cai, L. Li, J. Ren, L. Qiu, H. Lin and H. Peng, *J. Mater. Chem. A*, 2013, **1**, 258.
60 Z. Song, T. Ma, R. Tang, Q. Cheng, X. Wang, D. Krishnaraju, R. Panat, C. K. Chan, H. Yu and H. Jiang, *Nat. Commun.*, 2014, **5**, 3140.
61 L. Li, Z. Wu, S. Yuan and X.-B. B. Zhang, *Energy Environ. Sci.*, 2014, **7**, 2101.
62 S. Zhai, H. E. Karahan, L. Wei, Q. Qian, A. T. Harris, A. I. Minett, S. Ramakrishna, A. K. Ng and Y. Chen, *Energy Storage Mater.*, 2016, **3**, 123.
63 T. Lv, Y. Yao, N. Li and T. Chen, *Nano Today*, 2016, **11**, 644.
64 X. Lu, M. Yu, G. Wang, Y. Tong and Y. Li, *Energy Environ. Sci.*, 2014, **7**, 2160.
65 M.-S. Balogun, W. Qiu, W. Wang, P. Fang, X. Lu and Y. Tong, *J. Mater. Chem. A*, 2015, **3**, 1364–1387.
66 X. Zhang, H. Zhang, Z. Lin, M. Yu, X. Lu and Y. Tong, *Sci. China Mater.*, 2016, **59**, 475–494.
67 K. Fu, J. Cheng, T. Li and L. Hu, *ACS Energy Lett.*, 2016, **1**, 1065–1079.
68 L. Mao, Q. Meng, A. Ahmad and Z. Wei, *Adv. Energy Mater.*, 2017, 1700535.
69 Y. Li and J. Lu, *ACS Energy Lett.*, 2017, **2**, 1370.
70 A. Sumboja, X. Ge, Y. Zong and Z. Liu, *Funct. Mater. Lett.*, 2016, **9**, 1630001.
71 J. Fu, D. U. Lee, F. M. Hassan, L. Yang, Z. Bai, M. G. Park and Z. Chen, *Adv. Mater.*, 2015, **27**, 5617.
72 J. Fu, F. M. Hassan, J. Li, D. U. Lee, A. R. Ghannoum, G. Lui, M. A. Hoque and Z. Chen, *Adv. Mater.*, 2016, **28**, 6421.
73 J. Fu, J. Zhang, X. Song, H. Zarrin, X. Tian, J. Qiao, L. Rasen, K. Li and Z. Chen, *Energy Environ. Sci.*, 2016, **9**, 663.
74 Q. Liu, Y. Wang, L. Dai and J. Yao, *Adv. Mater.*, 2016, **28**, 3000.
75 S. Suren and S. Kheawhom, *J. Electrochem. Soc.*, 2016, **163**, A846.
76 Z. Wang, X. Meng, Z. Wu and S. Mitra, *J. Energy Chem.*, 2016, **26**, 129.
77 J. Zhang, J. Fu, X. Song, G. Jiang, H. Zarrin, P. Xu, K. Li, A. Yu and Z. Chen, *Adv. Energy Mater.*, 2016, **6**, 1600476.
78 C.-Y. Su, H. Cheng, W. Li, Z.-Q. Liu, N. Li, Z. Hou, F.-Q. Bai, H.-X. Zhang and T.-Y. Ma, *Adv. Energy Mater.*, 2017, **7**, 1602420.
79 M. Yu, Z. Wang, C. Hou, Z. Wang, C. Liang, C. Zhao, Y. Tong, X. Lu and S. Yang, *Adv. Mater.*, 2017, 1602868.
80 X. Chen, B. Liu, C. Zhong, Z. Liu, J. Liu, L. Ma, Y. Deng, X. Han, T. Wu, W. Hu and J. Lu, *Adv. Energy Mater.*, 2017, 1700779.
81 Z. Li, M. Shao, Q. Yang, Y. Tang, M. Wei, D. G. Evans and X. Duan, *Nano Energy*, 2017, **37**, 98.
82 Q.-C. Liu, L. Li, J.-J. Xu, Z.-W. Chang, D. Xu, Y.-B. Yin, X.-Y. Yang, T. Liu, Y.-S. Jiang, J.-M. Yan and X.-B. Zhang, *Adv. Mater.*, 2015, **27**, 8095.
83 W.-B. Luo, S.-L. Chou, J.-Z. Wang, Y.-M. Kang, Y.-C. Zhai and H.-K. Liu, *Chem. Commun.*, 2015, **51**, 8269.
84 Q. Liu, J. Xu, Z. Chang, D. Xu, Y. Yin, X. Yang, T. Liu, Y. Jiang, J. Yan and X. Zhang, *Part. Part. Syst. Charact.*, 2016, **33**, 500.
85 Q.-C. Liu, J.-J. Xu, D. Xu and X.-B. Zhang, *Nat. Commun.*, 2015, **6**, 7892.
86 H. Xue, S. Wu, J. Tang, H. Gong, P. He, J. He and H. Zhou, *ACS Appl. Mater. Interfaces*, 2016, **8**, 8427.
87 L. Wang, Y. Zhang, J. Pan and H. Peng, *J. Mater. Chem. A*, 2016, **4**, 13419.
88 X. Yang, J. Xu, D. Bao, Z. Chang, D. Liu, Y. Zhang and X.-B. Zhang, *Adv. Mater.*, 2017, **29**, 1700378.
89 J. Park, M. Park, G. Nam, J. Lee and J. Cho, *Adv. Mater.*, 2015, **27**, 1396.
90 Y. Xu, Y. Zhang, Z. Guo, J. Ren, Y. Wang and H. Peng, *Angew. Chemie Int. Ed.*, 2015, **54**, 15390.
91 F. Meng, H. Zhong, D. Bao, J. Yan and X. Zhang, *J. Am. Chem.*

Soc., 2016, **138**, 10226.
92 Y. Zhang, L. Wang, Z. Guo, Y. Xu, Y. Wang and H. Peng, *Angew. Chemie Int. Ed.*, 2016, **55**, 4487.
93 T. Liu, Q.-C. Liu, J.-J. Xu and X.-B. Zhang, *Small*, 2016, **12**, 3101.
94 X.-J. Lin, Q. Kang, Z. Zhang, R. Liu, Y. Li, Z. Huang, X. Feng, Y. Ma and W. Huang, *J. Mater. Chem. A*, 2017, **5**, 3638.
95 Q.-C. Liu, T. Liu, D.-P. Liu, Z.-J. Li, X.-B. Zhang and Y. Zhang, *Adv. Mater.*, 2016, **28**, 8413.
96 N. Mahmood, T. Tang and Y. Hou, *Adv. Energy Mater.*, 2016, **6**, 1600374.
97 T. Liu, J.-J. Xu, Q.-C. Liu, Z.-W. Chang, Y.-B. Yin, X.-Y. Yang and X.-B. Zhang, *Small*, 2017, **13**, 1602952.
98 E. Quartarone and P. Mustarelli, *Chem. Soc. Rev.*, 2011, **40**, 2525.
99 Y.-S. Hu, *Nat. Energy*, 2016, **1**, 16042.
100 S. Gu, R. Cai, T. Luo, Z. Chen, M. Sun, Y. Liu, G. He and Y. Yan, *Angew. Chemie Int. Ed.*, 2009, **48**, 6499.
101 S. Gu, J. Wang, R. B. Kaspar, Q. Fang, B. Zhang, E. Bryan Coughlin and Y. Yan, *Sci. Rep.*, 2015, **5**, 11668.
102 Y.-J. Wang, J. Qiao, R. Baker and J. Zhang, *Chem. Soc. Rev.*, 2013, **42**, 5768.
103 X. Zhu, H. Yang, Y. Cao and X. Ai, *Electrochim. Acta*, 2004, **49**, 2533.
104 A. Lewandowski, *Solid State Ionics*, 2000, **133**, 265.
105 N. Vassal, E. Salmon and J. F. Fauvarque, *Electrochim. Acta*, 2000, **45**, 1527.
106 R. Othman, W. J. Basirun, A. H. Yahaya and A. K. Arof, *J. Power Sources*, 2001, **103**, 34.
107 C. C. Yang and S. J. Lin, *J. Power Sources*, 2002, **112**, 497.
108 A. A. Mohamad, *J. Power Sources*, 2006, **159**, 752.
109 A. Manthiram, X. Yu and S. Wang, *Nat. Rev. Mater.*, 2017, **2**, 16103.
110 C. Sun, J. Liu, Y. Gong, D. P. Wilkinson and J. Zhang, *Nano Energy*, 2017, **33**, 363.
111 H. Kitaura and H. Zhou, *Adv. Energy Mater.*, 2012, **2**, 889.
112 H. Kitaura and H. Zhou, *Energy Environ. Sci.*, 2012, **5**, 9077.
113 X. B. Zhu, T. S. Zhao, Z. H. Wei, P. Tan and G. Zhao, *Energy Environ. Sci.*, 2015, **8**, 2782.
114 J. Yi and H. Zhou, *ChemSusChem*, 2016, **9**, 2391.
115 J. Yi, S. Guo, P. He and H. Zhou, *Energy Environ. Sci.*, 2017, **10**, 860.
116 C. Wu, C. Liao, T. Li, Y. Shi, J. Luo, L. Li and J. Yang, *J. Mater. Chem. A*, 2016, **4**, 15189.
117 G. A. Elia and J. Hassoun, *Solid State Ionics*, 2016, **287**, 22.
118 G. A. Elia and J. Hassoun, *Sci. Rep.*, 2015, **5**, 12307.
119 J. Yi, X. Liu, S. Guo, K. Zhu, H. Xue and H. Zhou, *ACS Appl. Mater. Interfaces*, 2015, **7**, 23798.
120 J. Zhang, B. Sun, X. Xie, K. Kretschmer and G. Wang, *Electrochim. Acta*, 2015, **183**, 56.
121 K.-N. Jung, J.-I. Lee, J.-H. Jung, K.-H. Shin and J.-W. Lee, *Chem. Commun.*, 2014, **50**, 5458.
122 Z. Gadjourova, Y. G. Andreev, D. P. Tunstall and P. G. Bruce, *Nature*, 2001, **412**, 520.
123 M. Balaish, E. Peled, D. Golodnitsky and Y. Ein-Eli, *Angew. Chemie Int. Ed.*, 2014, **54**, 436.
124 J. Li, Y. Lin, H. Yao, C. Yuan and J. Liu, *ChemSusChem*, 2014, **7**, 1901.
125 N. Bonnet-Mercier, R. A. Wong, M. L. Thomas, A. Dutta, K. Yamanaka, C. Yogi, T. Ohta and H. R. Byon, *Sci. Rep.*, 2014, **4**, 7127.
126 K. Fu, Y. Gong, J. Dai, A. Gong, X. Han, Y. Yao, C. Wang, Y. Wang, Y. Chen, C. Yan, Y. Li, E. D. Wachsman and L. Hu, *Proc. Natl. Acad. Sci.*, 2016, **113**, 7094.
127 Y.-C. Jung, S.-M. Lee, J.-H. Choi, S. S. Jang and D.-W. Kim, *J. Electrochem. Soc.* , 2015, **162**, A704.
128 F. Li, D.-M. Tang, T. Zhang, K. Liao, P. He, D. Golberg, A. Yamada and H. Zhou, *Adv. Energy Mater.*, 2015, **5**, 1500294.
129 J. Jung, K. Song, Y. Bae, S. Il Choi, M. Park, E. Cho, K. Kang and Y. M. Kang, *Nano Energy*, 2015, **18**, 71.
130 H. D. Lim, H. Song, J. Kim, H. Gwon, Y. Bae, K. Y. Park, J. Hong, H. Kim, T. Kim, Y. H. Kim, X. Lepró, R. Ovalle-Robles, R. H. Baughman and K. Kang, *Angew. Chemie Int. Ed.*, 2014, **53**, 3926.
131 Y. Guo, H. Li and T. Zhai, *Adv. Mater.*, 2017, **29**, 1700007.
132 H.-J. Shin, W.-J. Kwak, D. Aurbach and Y.-K. Sun, *Adv. Funct. Mater.*, 2017, **27**, 1605500.
133 C. Yang, Z. Zhang, Z. Tian, K. Zhang, J. Li and Y. Lai, *J. Electrochem. Soc.*, 2016, **163**, A1836.
134 S. J. Banik and R. Akolkar, *J. Electrochem. Soc.*, 2013, **160**, D519.
135 S. J. Banik and R. Akolkar, *Electrochim. Acta*, 2015, **179**, 475.
136 S. Lee, K. Kim and C. Yi, *Bull. Korean Chem. Soc.*, 2013, **34**, 717.
137 Z. Liu, S. Zein El Abedin and F. Endres, *J. Solid State Electrochem.*, 2014, **18**, 2683.
138 W. Xu, J. Wang, F. Ding, X. Chen, E. Nasybulin, Y. Zhang and J.-G. Zhang, *Energy Environ. Sci.*, 2014, **7**, 513.
139 O. Crowther and A. C. West, *J. Electrochem. Soc.*, 2008, **115**, A806.
140 T. Nishida, K. Nishikawa, M. Rosso and Y. Fukunaka, *Electrochim. Acta*, 2013, **100**, 333.
141 F. Ding, W. Xu, X. Chen, J.-G. Zhang, M. H. Engelhard, Y. Zhang, B. R. Johnson, J. V. Crum, T. a. Blake, X. Liu and J.-G. Zhang, *J. Electrochem. Soc.*, 2013, **160**, A1894.
142 M. S. Park, S. B. Ma, D. J. Lee, D. Im, S.-G. Doo and O. Yamamoto, *Sci. Rep.*, 2014, **4**, 3815.
143 N.-S. Choi, B. Koo, J.-T. Yeon, K. T. Lee and D.-W. Kim, *Electrochim. Acta*, 2011, **56**, 7249.
144 T. Tatsuma, M. Taguchi, M. Iwaku, T. Sotomura and N. Oyama, *J. Electroanal. Chem.*, 1999, **472**, 142.
145 C. Brissot, M. Rosso, J. N. Chazalviel, P. Baudry and S. Lascaud, *Electrochim. Acta*, 1998, **43**, 1569.
146 C. Brissot, *J. Electrochem. Soc.*, 1999, **146**, 4393.
147 C. Brissot, M. Rosso, J. N. Chazalviel and S. Lascaud, *J. Power Sources*, 1999, **81**, 925.
148 M. Rosso, C. Brissot, A. Teyssot, M. Dollé, L. Sannier, J. M. Tarascon, R. Bouchet and S. Lascaud, *Electrochim. Acta*, 2006, **51**, 5334.
149 C. Monroe and J. Newman, *J. Electrochem. Soc.*, 2005, **152**, A396.
150 R. Khurana, J. L. Schaefer, L. A. Archer and G. W. Coates, *J. Am. Chem. Soc.*, 2014, **136**, 7395.
151 S. Liu, N. Imanishi, T. Zhang, A. Hirano, Y. Takeda, O. Yamamoto and J. Yang, *J. Power Sources*, 2010, **195**, 6847.
152 S. Liu, H. Wang, N. Imanishi, T. Zhang, A. Hirano, Y. Takeda, O. Yamamoto and J. Yang, *J. Power Sources*, 2011, **196**, 7681.
153 S. Choudhury, R. Mangal, A. Agrawal and L. A. Archer, *Nat. Commun.*, 2015, **6**, 10101.
154 J.-J. Xu, Q.-C. Liu, Y. Yu, J. Wang, J.-M. Yan and X.-B. Zhang, *Adv. Mater.*, 2017, **29**, 1606552.
155 H. Song, H. Deng, C. Li, N. Feng, P. He and H. Zhou, *Small Methods*, 2017, **1**, 1700135.
156 P. Tan, W. Shyy and T. Zhao, *Sci. Bull.*, 2015, **60**, 975.
157 T. Zhang and H. Zhou, *Angew. Chemie Int. Ed.*, 2012, **51**, 11062.

158 A. Eftekhari and B. Ramanujam, *J. Mater. Chem. A*, 2017, **5**, 7710.
159 Y. Chen, S. a Freunberger, Z. Peng, O. Fontaine and P. G. Bruce, *Nat. Chem.*, 2013, **5**, 489.
160 B. J. Bergner, A. Schürmann, K. Peppler, A. Garsuch and J. Janek, *J. Am. Chem. Soc.*, 2014, **136**, 15054.
161 T. Zhang, K. Liao, P. He and H. Zhou, *Energy Environ. Sci.*, 2016, **9**, 1024.
162 D. Hirshberg, W.-J. Kwak, D. Sharon, M. Afri, A. A. Frimer, H.-G. Jung, D. Aurbach and Y.-K. Sun, *Energy Environ. Sci.*, 2016, **9**, 2334.
163 D. Sun, Y. Shen, W. Zhang, L. Yu, Z. Yi, W. Yin, D. Wang, Y. Huang, J. Wang, D. Wang and J. B. Goodenough, *J. Am. Chem. Soc.*, 2014, **136**, 8941.
164 J. Yi, S. Wu, S. Bai, Y. Liu, N. Li and H. Zhou, *J. Mater. Chem. A*, 2016, **4**, 2403.
165 D. Guo, X. Yu, W. Shi, Y. Luo, Q. Li and T. Wang, *J. Mater. Chem. A*, 2014, **2**, 8833.
166 T. Y. Ma, J. Ran, S. Dai, M. Jaroniec and S. Z. Qiao, *Angew. Chemie Int. Ed.*, 2015, **54**, 4646.
167 H.-D. Lim, Y. S. Yun, S. Y. Cho, K.-Y. Park, M. Y. Song, H.-J. Jin and K. Kang, *Carbon*, 2016, **114**, 311.
168 P. Tan, W. Shyy, T. S. Zhao, X. B. Zhu and Z. H. Wei, *J. Mater. Chem. A*, 2015, **3**, 19042.
169 P. Tan, W. Shyy, Z. H. Wei, L. An and T. S. Zhao, *Electrochim. Acta*, 2014, **147**, 1.
170 Z. Jian, P. Liu, F. Li, P. He, X. Guo, M. Chen and H. Zhou, *Angew. Chemie Int. Ed.*, 2014, **53**, 442.
171 G. Q. Zhang, J. P. Zheng, R. Liang, C. Zhang, B. Wang, M. Hendrickson and E. J. Plichta, *J. Electrochem. Soc.* , 2010, **157**, A953.
172 H. D. Lim, K. Y. Park, H. Song, E. Y. Jang, H. Gwon, J. Kim, Y. H. Kim, M. D. Lima, R. O. Robles, X. Lepró, R. H. Baughman and K. Kang, *Adv. Mater.*, 2013, **25**, 1348.
173 N. Gupta, T. Toh, M. W. Fatt, S. Mhaisalkar and M. Srinivasan, *J. Solid State Electrochem.*, 2012, **16**, 1585.
174 Y. Chen, F. Li, D.-M. Tang, Z. Jian, C. Liu, D. Golberg, A. Yamada and H. Zhou, *J. Mater. Chem. A*, 2013, **1**, 13076.
175 H.-D. Lim, H. Song, H. Gwon, K.-Y. Park, J. Kim, Y. Bae, H. Kim, S.-K. Jung, T. Kim, Y. H. Kim, X. Lepró, R. Ovalle-Robles, R. H. Baughman and K. Kang, *Energy Environ. Sci.*, 2013, **6**, 3570.
176 S. Martinez Crespiera, D. Amantia, E. Knipping, C. Aucher, L. Aubouy, J. Amici, J. Zeng, U. Zubair, C. Francia and S. Bodoardo, *J. Appl. Electrochem.*, 2017, **47**, 497.
177 D. Ji, S. Peng, D. Safanama, H. Yu, L. Li, G. Yang, X. Qin, S. Madhavi, S. Adams and S. Ramakrishna, *Chem. Mater.*, 2017, **29**, 1665.
178 Y.-B. Yin, J.-J. Xu, Q.-C. Liu and X.-B. Zhang, *Adv. Mater.*, 2016, **28**, 7494.
179 H. Xue, X. Mu, J. Tang, X. Fan, H. Gong, T. Wang, J. He and Y. Yamauchi, *J. Mater. Chem. A*, 2016, **4**, 9106.
180 D. Y. Kim, M. Kim, D. W. Kim, J. Suk, O. O. Park and Y. Kang, *Carbon*, 2015, **93**, 625.
181 Y. Zhu, S. Murali, W. Cai, X. Li, J. W. Suk, J. R. Potts and R. S. Ruoff, *Adv. Mater.*, 2010, **22**, 3906.
182 Y. Sun, Q. Wu and G. Shi, *Energy Environ. Sci.*, 2011, **4**, 1113.
183 Y. Lin, B. Moitoso, C. Martinez-Martinez, E. D. Walsh, S. D. Lacey, J.-W. Kim, L. Dai, L. Hu and J. W. Connell, *Nano Lett.*, 2017, **17**, 3252.
184 T. Cetinkaya, S. Ozcan, M. Uysal, M. O. Guler and H. Akbulut, *J. Power Sources*, 2014, **267**, 140.
185 M. Kim, D. Y. Kim, Y. Kang and O. O. Park, *RSC Adv.*, 2015, **5**, 3299.
186 S. Ozcan, M. Tokur, T. Cetinkaya, A. Guler, M. Uysal, M. O. Guler and H. Akbulut, *Solid State Ionics*, 2016, **286**, 34.
187 K. H. Kangasniemi, D. A. Condit and T. D. Jarvi, *J. Electrochem. Soc.* , 2004, **151**, E125.
188 X. Wang, W. Li, Z. Chen, M. Waje and Y. Yan, *J. Power Sources*, 2006, **158**, 154.
189 B. D. McCloskey, A. Speidel, R. Scheffler, D. C. Miller, V. Viswanathan, J. S. Hummelshøj, J. K. Nørskov and A. C. Luntz, *J. Phys. Chem. Lett.*, 2012, **3**, 997.
190 D. M. Itkis, D. A. Semenenko, E. Y. Kataev, A. I. Belova, V. S. Neudachina, A. P. Sirotina, M. Hävecker, D. Teschner, A. Knop-Gericke, P. Dudin, A. Barinov, E. A. Goodilin, Y. Shao-Horn and L. V. Yashina, *Nano Lett.*, 2013, **13**, 4697.
191 M. M. Ottakam Thotiyl, S. A. Freunberger, Z. Peng and P. G. Bruce, *J. Am. Chem. Soc.*, 2013, **135**, 494.
192 P. Tan, W. Shyy, M. C. Wu, Y. Y. Huang and T. S. Zhao, *J. Power Sources*, 2016, **326**, 303.
193 J.-S. Lee, T. Lee, H.-K. Song, J. Cho and B.-S. Kim, *Energy Environ. Sci.*, 2011, **4**, 4148.
194 L. Leng, X. Zeng, H. Song, T. Shu, H. Wang and S. Liao, *J. Mater. Chem. A*, 2015, **3**, 15626.
195 A. Riaz, K.-N. Jung, W. Chang, S.-B. Lee, T.-H. Lim, S.-J. Park, R.-H. Song, S. Yoon, K.-H. Shin and J.-W. Lee, *Chem. Commun.*, 2013, **49**, 5984.
196 K. Liao, T. Zhang, Y. Wang, F. Li, Z. Jian, H. Yu and H. Zhou, *ChemSusChem*, 2015, **8**, 1429.
197 S. T. Kim, N.-S. Choi, S. Park and J. Cho, *Adv. Energy Mater.*, 2015, **5**, 1401030.
198 Y. Yu, B. Zhang, Z. L. Xu, Y. B. He and J. K. Kim, *Solid State Ionics*, 2014, **262**, 197.
199 W. Bin Luo, X. W. Gao, S. L. Chou, J. Z. Wang and H. K. Liu, *Adv. Mater.*, 2015, **27**, 6862.
200 F. Li, D. M. Tang, Y. Chen, D. Golberg, H. Kitaura, T. Zhang, A. Yamada and H. Zhou, *Nano Lett.*, 2013, **13**, 4702.
201 D. U. Lee, J.-Y. Choi, K. Feng, H. W. Park and Z. Chen, *Adv. Energy Mater.*, 2014, **4**, 1301389.
202 G. M. Veith and N. J. Dudney, *J. Electrochem. Soc.* , 2011, **158**, A658.
203 Z. Peng, S. A. Freunberger, Y. Chen and P. G. Bruce, *Science*, 2012, **337**, 563.
204 M. Hilder, B. Winther-Jensen and N. B. Clark, *J. Power Sources*, 2009, **194**, 1135.
205 K. R. Yoon, J.-W. Jung and I.-D. Kim, *ChemNanoMat*, 2016, **2**, 616.
206 K. R. Yoon, G. Y. Lee, J. W. Jung, N. H. Kim, S. O. Kim and I. D. Kim, *Nano Lett.*, 2016, **16**, 2076.
207 P. Li, J. Zhang, Q. Yu, J. Qiao, Z. Wang, D. Rooney, W. Sun and K. Sun, *Electrochim. Acta*, 2015, **165**, 78.
208 F. Lu, Y. Wang, C. Jin, F. Li, R. Yang and F. Chen, *J. Power Sources*, 2015, **293**, 726.
209 Q. Li, P. Xu, B. Zhang, H. Tsai, J. Wang, H.-L. Wang and G. Wu, *Chem. Commun.*, 2013, **49**, 10838.
210 J.-W. Jung, H.-G. Im, D. Lee, S. Yu, J.-H. Jang, K. R. Yoon, Y. H. Kim, J. B. Goodenough, J. Jin, I.-D. Kim and B.-S. Bae, *ACS Energy Lett.*, 2017, **2**, 673.
211 P. Tan, H. R. Jiang, X. B. Zhu, L. An, C. Y. Jung, M. C. Wu, L. Shi, W. Shyy and T. S. Zhao, *Appl. Energy*, 2017, **204**, 780.
212 S. A. Freunberger, Y. Chen, Z. Peng, J. M. Griffin, L. J. Hardwick, F. Bardé, P. Novák and P. G. Bruce, *J. Am. Chem. Soc.*, 2011, **133**, 8040.
213 S. Ma, Y. Wu, J. Wang, Y. Zhang, Y. Zhang, X. Yan, Y. Wei, P.

Liu, J. Wang, K. Jiang, S. Fan, Y. Xu and Z. Peng, *Nano Lett.*, 2015, **15**, 8084.
214 J. Lu, L. Li, J. B. Park, Y. K. Sun, F. Wu and K. Amine, *Chem. Rev.*, 2014, **114**, 5611.
215 L. A. Adams, S. D. Poynton, C. Tamain, R. C. T. Slade and J. R. Varcoe, *ChemSusChem*, 2008, **1**, 79.
216 J.-F. Drillet, F. Holzer, T. Kallis, S. Muller and V. M. Schmidt, *Phys. Chem. Chem. Phys.*, 2001, **3**, 368.
217 H.-H. Cheng and C.-S. Tan, *J. Power Sources*, 2006, **162**, 1431.
218 S. K. Das, S. Xu, A.-H. Emwas, Y. Y. Lu, S. Srivastava and L. a. Archer, *Energy Environ. Sci.*, 2012, **5**, 8927.
219 P. Tan, L. Shi, W. Shyy and T. Zhao, *Energy Technol.*, 2016, **4**, 393.
220 E. Joseph Nemanick and R. P. Hickey, *J. Power Sources*, 2014, **252**, 248.
221 J.-L. Shui, J. S. Okasinski, P. Kenesei, H. a Dobbs, D. Zhao, J. D. Almer and D.-J. Liu, *Nat. Commun.*, 2013, **4**, 2255.
222 S. Huang, Z. Cui, N. Zhao, J. Sun and X. Guo, *Electrochim. Acta*, 2016, **191**, 473.
223 R. Black, S. H. Oh, J. H. Lee, T. Yim, B. Adams and L. F. Nazar, *J. Am. Chem. Soc.*, 2012, **134**, 2902.
224 R. S. Assary, J. Lu, P. Du, X. Luo, X. Zhang, Y. Ren, L. A. Curtiss and K. Amine, *ChemSusChem*, 2013, **6**, 51.
225 S. Meini, N. Tsiouvaras, K. U. Schwenke, M. Piana, H. Beyer, L. Lange and H. A. Gasteiger, *Phys. Chem. Chem. Phys.*, 2013, **15**, 11478.
226 C. Ling, R. Zhang, K. Takechi and F. Mizuno, *J. Phys. Chem. C*, 2014, **118**, 26591.
227 G. Wang, L. Huang, S. Liu, J. Xie, S. Zhang, P. Zhu, G. Cao and X. Zhao, *ACS Appl. Mater. Interfaces*, 2015, **7**, 23876.
228 Y. Shen, D. Sun, L. Yu, W. Zhang, Y. Shang, H. Tang, J. Wu, A. Cao and Y. Huang, *Carbon*, 2013, **62**, 288.
229 B. G. Kim, J. S. Kim, J. Min, Y. H. Lee, J. H. Choi, M. C. Jang, S. A. Freunberger and J. W. Choi, *Adv. Funct. Mater.*, 2016, **26**, 1747.
230 S. Wu, J. Yi, K. Zhu, S. Bai, Y. Liu, Y. Qiao, M. Ishida and H. Zhou, *Adv. Energy Mater.*, 2017, **7**, 1601759.
231 J.-G. Zhang, D. Wang, W. Xu, J. Xiao and R. E. Williford, *J. Power Sources*, 2010, **195**, 4332.
232 D. Wang, J. Xiao, W. Xu and J.-G. Zhang, *J. Electrochem. Soc.* , 2010, **157**, A760.
233 J. Zhang, W. Xu, X. Li and W. Liu, *J. Electrochem. Soc.* , 2010, **157**, A940.
234 J. Zhang, W. Xu and W. Liu, *J. Power Sources*, 2010, **195**, 7438.
235 O. Crowther, D. Keeny, D. M. Moureau, B. Meyer, M. Salomon and M. Hendrickson, *J. Power Sources*, 2012, **202**, 347.
236 J. Amici, M. Alidoost, C. Francia, S. Bodoardo, S. Martinez Crespiera, D. Amantia, M. Biasizzo, F. Caldera and F. Trotta, *Chem. Commun.*, 2016, **52**, 13683.
237 X. B. Zhu, T. S. Zhao, Z. H. Wei, P. Tan and L. An, *Energy Environ. Sci.*, 2015, **8**, 3745.
238 F. Li, S. Wu, D. Li, T. Zhang, P. He, A. Yamada and H. Zhou, *Nat. Commun.*, 2015, **6**, 7843.
239 S. Wu, J. Tang, F. Li, X. Liu, Y. Yamauchi, M. Ishida and H. Zhou, *Adv. Funct. Mater.*, 2016, **26**, 3291.
240 P. Tan, Z. H. Wei, W. Shyy, T. S. Zhao and X. B. Zhu, *Energy Environ. Sci.*, 2016, **9**, 1783.
241 P. Tan, W. Shyy, T. S. Zhao, R. H. Zhang and X. B. Zhu, *Appl. Energy*, 2016, **182**, 569.
242 Y. Liu, R. Wang, Y. Lyu, H. Li and L. Chen, *Energy Environ. Sci.*, 2014, **7**, 677.
243 Z. Xie, X. Zhang, Z. Zhang and Z. Zhou, *Adv. Mater.*, 2017, **29**, 1605891.
244 X. Hu, Z. Li and J. Chen, *Angew. Chemie*, 2017, **129**, 5879.
245 Y. Qiao, J. Yi, S. Wu, Y. Liu, S. Yang, P. He and H. Zhou, *Joule*, 2017, **1**, 1.
246 X. Zhang, Q. Zhang, Z. Zhang, Y. Chen, Z. Xie, J. Wei and Z. Zhou, *Chem. Commun.*, 2015, **51**, 14636.
247 Z. Zhang, Q. Zhang, Y. Chen, J. Bao, X. Zhou, Z. Xie, J. Wei and Z. Zhou, *Angew. Chemie Int. Ed.*, 2015, **54**, 6550.
248 S. Yang, Y. Qiao, P. He, Y. Liu, Z. Cheng, J. Zhu and H. Zhou, *Energy Environ. Sci.*, 2017, **10**, 972.
249 H.-K. Lim, H.-D. Lim, K.-Y. Park, D.-H. Seo, H. Gwon, J. Hong, W. A. Goddard ,III, H. Kim and K. Kang, *J. Am. Chem. Soc.*, 2013, **135**, 9733.
250 S. Yang, P. He and H. Zhou, *Energy Environ. Sci.*, 2016, **9**, 1650.
251 R. Wang, X. Yu, J. Bai, H. Li, X. Huang, L. Chen and X. Yang, *J. Power Sources*, 2012, **218**, 113.
252 M. Hong, H. C. Choi and H. R. Byon, *Chem. Mater.*, 2015, **27**, 2234.
253 S. Tong, M. Zheng, Y. Lu, Z. Lin, J. Li, X. Zhang, Y. Shi, P. He and H. Zhou, *J. Mater. Chem. A*, 2015, **3**, 16177.
254 S. Song, W. Xu, J. Zheng, L. Luo, M. H. Engelhard, M. E. Bowden, B. Liu, C. Wang and J.-G. Zhang, *Nano Lett.*, 2017, **17**, 1417.
255 J. B. Park, J. Hassoun, H. G. Jung, H. S. Kim, C. S. Yoon, I. H. Oh, B. Scrosati and Y. K. Sun, *Nano Lett.*, 2013, **13**, 2971.
256 P. Tan, W. Shyy, T. S. Zhao, Z. H. Wei and L. An, *J. Power Sources*, 2015, **278**, 133.
257 F. Mohazabrad, F. Wang and X. Li, *ACS Appl. Mater. Interfaces*, 2017, **9**, 15459.
258 P. Tan, W. Kong, Z. Shao, M. Liu and M. Ni, *Prog. Energy Combust. Sci.*, 2017, **62**, 155.